2015

Dynamic Behavior of Materials Subjected to Extreme Environments

Christopher S. Shillings
University of Rhode Island, shill52@my.uri.edu

DYNAMIC BEHAVIOR OF MATERIALS SUBJECTED TO EXTREME ENVIRONMENTS

BY

CHRISTOPHER S. SHILLINGS

A THESIS SUBMITTED IN PARTIAL FULFILLENT OF THE REQUIREMENTS FOR THE DEGREE OF MASTER OF SCIENCE IN MECHANICAL ENGINEERING AND APPLIED MECHANICS

UNIVERSITY OF RHODE ISLAND

2015

MASTER OF SCIENCE THESIS

OF

CHRISTOPHER S. SHILLINGS

APPROVED:

Thesis Committee:

Major Professor **Arun Shukla**

James LeBlanc

James Miller

Nasser H. Zawia
DEAN OF THE GRADUATE SCHOOL

UNIVERSITY OF RHODE ISLAND

2015

ABSTRACT

An experimental investigation was conducted to understand the fundamental physics of various dynamic events. The study seeks to understand the shock response of composite materials after long-term exposure to accelerated aging conditions, polyurea coated composites subjected to near field underwater explosions, and the implosion behavior of brittle volumes.

First, the shock response of carbon/epoxy composites subjected to aggressive marine environments was explored. In order to simulate a prolonged submergence in oceanic conditions, an elevated temperature, salt water environment was created. The material was submerged in a 3.5%, 65°C salt solution for 0, 30 and 60 days. Tensile and four point bend experiments were performed for each case to determine quasi-static properties, while shock tube experiments were used to determine dynamic behavior of the material. After 30 days of submergence, the mechanical properties of the composite diminished. Furthermore, after an additional 30 days of submergence, the 60 day submerged specimens displayed similar quasi-static and dynamic mechanical behavior to the 30 day case.

Secondly, the transient response of polyurea coated E-Glass/Epoxy composites exposed to near field underwater explosions was investigated. The composite panels were positioned as a boundary between air and water, simulating a ship hull. Three types of panels were studied with varying thicknesses and material layups. The specimens are as follows: 0.762 mm thick with no coating, 1.524 mm with no coating and 0.762 mm composite with 0.762 mm polyurea coating. The 0.762 mm panel

served as the control sample while the 1.524 mm thick panels with and without coating were compared. In all cases, fully clamped panels were subjected to an underwater explosive charge with a 5 cm standoff distance. All panels displayed deflection, however the polyurea coated composite displayed a lower maximum deflection, with an adjusted weight parameter, than the 1.524 mm thick composite. Also, shearing at the fully clamped boundaries, leading to fluid penetration, did not occur when polyurea coated the composite panels.

Lastly, the implosion behavior of brittle volumes submerged in pressurized water was studied. The implodable volumes chosen in this study were polymethylmethacrylate (PMMA) tubing. Three geometries of tubing were chosen with an outer diameter of 25.4 mm and lengths of 76.2 mm, 152.4 mm and 228.6 mm. All specimens were placed within a confined vessel equipped with a viewing window for high speed photography. In all cases, pressure was increased at a quasi-static rate until the tubes dynamically collapsed. Experiments uncovered distinct fracture patterns and high crack velocity due to a biaxial loading condition.

ACKNOWLEDGEMENTS

First and foremost, I would like to express my gratitude to Dr. Arun Shukla for his guidance and support throughout my graduate studies. His knowledge and expertise has pushed my understanding of engineering beyond my own expectations. His patience and generosity is something one could ever hope for in a mentor and is a tribute to his success as a researcher and most of all an individual. As a sophomore in my mechanical undergraduate studies I joined the lab with a limited knowledge of mechanical engineering and am leaving with a deeper understanding of the science and its applications. Dr. Shukla is epitome of a success in that his scientific contributions have furthered the field of solid mechanics; he has established a community, the DPML, which will thrive with the strong network of past and present students; and his vast amount of work will be the foundation for the growth of engineering at the University of Rhode Island. I am blessed and honored to have studied under the guidance of Dr. Arun Shukla.

I would also like to sincerely thank Dr. James LeBlanc and Dr. James Miller for serving as my committee members. Also a special thanks to Dr. D.M.L. Meyer for her guidance, enthusiasm for teaching and constant reminders to always check my units.

I would like to thank all of my lab mates in the Dynamic Photomechanics Laboratory: Mike Pinto, Prathmesh Parrikar, Helio Matos, Emad Makki, Craig Tilton, Laura Corvese, Erin Gauch, Shyamal Kishore, Nicholas DeNardo and Kim McCarthy. I would also like to acknowledge past DPML members: Sachin Gupta, Payam Fahr,

Nicholas Heeder, Chris O'Connell, Frank LiVolsi, Sandeep Abotula and Nate Gardner. With all of your help, guidance and support you made completing my master's degree possible, but most importantly you all kept my sanity intact. A special thanks to the mechanical engineering department and staff, especially Joe Gomez, Nancy Dubee, Dave Ferriera, Jim Byrnes, Rob D'Ambrosca and AJ Bothun.

I would also like to thank the financial support provided by the Naval Engineering Education Consortium (NEEC) Grant # 3003266434 and the Naval Undersea Warfare Center (Division Newport) Chief Technology Office. The financial support of the Naval Undersea Warfare Center (Division Newport) In-house Laboratory Independent Research program (ILIR) directed by Neil Dubois. The support of Dr. Y.D.S. Rajapakse of the Office of Naval Research under Grant Nos. N00014-10-1-0662 (University of Rhode Island) and N00014-14-WX00730 (Naval Undersea Warfare Center, Division Newport). And finally, the financial support provided by the Office of Naval Research Computational Mechanics Program managed by Dr. Stephen E. Turner under Grant No. N00014-12-1-0382

Last and certainly not least, I would like to thank my parents Curtis and Cynthia and my sister Rebecca. I could not have completed my studies without their endless love and support. Also I would like to thank my late dog and friend Miss Maggie Mae for helping me escape the stress of graduate work and understand life's toughest obstacles can be solved by going for a walk.

PREFACE

A series of experimental studies were performed to study the fundamental physics of various dynamic events. This work focuses on areas of naval interest including: the effects of aging on the mechanical properties of composite materials subjected to an in air blast, the underwater explosive resistance of a coated composite, and the implosion characteristics of a brittle cylinder submerged under critical hydrostatic pressure. The aim of this work is to expand upon the knowledge of such complex events and aid in the understanding of specific material responses under such extreme conditions. This thesis is prepared using the manuscript format.

Chapter 1 investigates the quasi-static and dynamic response of carbon/epoxy specimens before and after prolonged exposure in a salt solution at an elevated temperature. This section discusses the objective and motivation driving this work, the composite material properties, experimental theory and procedures, experiments performed, and lastly results with conclusions. The focus of this work is the accelerated aging theory coupled with submergence experimentation and the shock loading of the composite material before and after weathering. Additional computational analysis was performed to replicate shock loading scenarios.

Chapter 2 investigates the response of polyurea coated and non-coated E-Glass/Epoxy composite plates subjected to near field underwater explosion (UNDEX) loading. Similarly, this section discusses the objective and motivation driving this work, the materials studied experimental theory and procedures, experiments performed, and lastly results, followed by conclusions. The aim of this work is to

evaluate the transient response of the coated and non-coated panels during an underwater explosion event, then compare their performance, and observe the survivability of each panel via damage resistance.

Chapter 3 explores the implosion behavior of brittle cylinders under critical hydrostatic loading. Polymethylmethacrylate (PMMA) tubes are imploded within a confined region in order to view the crack propagation as the material undergoes brittle failure. Chapter 3 describes the specimen preparation, testing procedures to capture the pressure and visual history of the event, and both observational and pressure history followed by conclusions.

Table of Contents

List of Figures

CHAPTER 1

List of Tables

CHAPTER 1

CHAPTER 2

CHAPTER 3

CHAPTER 1

SHOCK RESPONSE OF COMPOSITE MATERIALS SUBJECTED TO AGGRESSIVE MARINE ENVRINONMENTS: AN EXPERIMENTAL AND COMPUTATIONAL INVESTIGATION

by

Christopher Shillings, James LeBlanc, Craig Tilton, Laura Corvese, Arun Shukla

Prepared for submission to Experimental Mechanics

Corresponding Author: Christopher Shillings

University of Rhode Island

Mechanical, Industrial and Systems Engineering

92 Upper College Road, Kingston, RI 02881

Phone: 401 – 864 – 9443

Email Address: shill52@my.uri.edu

Abstract

The shock response of carbon/epoxy composite panels subjected to an aggressive marine environment was explored to determine the effects of significant weathering on the dynamic mechanical response of the material. Carbon/epoxy was chosen due to its significance in recent naval applications and its relevance in future designs. Specimens were submerged in a 3.5 % salt solution for 0, 30 and 60 days, simulating a marine environment. The temperature was maintained at 65°C to accelerate diffusion into the composite matrix, thus accelerating the weathering process. Tensile and four point bend experiments were performed to determine quasi-static behavior of the composite material, while shock tube experiments were performed to investigate the dynamic behavior. All experiments were conducted for each exposure time.

From quasi-static experimentation it was determined that after 30 and 60 days of submergence the tensile modulus decreased by 11% and 11% respectively, the ultimate tensile strength decreased by 12% and 13%, the ultimate flexural strength decreased by 22% and 23%.

The weathered (30 and 60 days) and non-weathered (0 day) specimens displayed dramatically different behavior after being subjected to a dynamic shock loading. The composite specimens were simply supported and subjected to a controlled and concentrated air blast loading using a shock tube. Non-weathered specimens displayed an average maximum deflection of 20 mm and recovered elastically. Weathered specimens (30 and 60 days) showed similar transient behavior

as the 0 day case, however at ~1 ms, displayed cracking on the compression face followed by catastrophic through thickness cracking.

Introduction

Within the navy there is an interest in using composite materials for the construction of vehicles due to its high strength to weight ratio. The use of composite materials in naval applications dates back to the 1940s, when small river patrol boats were constructed entirely of the material. Composite materials were also used to create smaller parts within ships such as fins, rudders, and torpedo tubes, reducing the weight of the vessels [1]. As technology advanced, large ship hulls were able to be fabricated from composite materials. Today, Visby Class Corvettes longer than 70 meters are made entirely of composites [1].

The use of composite materials is appealing to the navy not only due to their strength to weight ratio, which can increase fuel range and economy, but also because of their abilities to aid in keeping the vehicle stealth. Composite materials have low infrared, magnetic, and radar cross sectional signatures, keeping navy vessels hidden from enemies. Additionally, composites provide electromagnetic shielding and have good noise dampening properties [1]. Due to these advantages, unmanned vehicles, such as the Manta and Deepglider UUVs , as well as minesweepers, are being constructed of composite materials. However, composites have lower impact resistance than steels and can degrade due to the undersea environment. Thus, studying the effects of the degradation of mechanical properties of composite materials, in particular on shock response, is of high priority.

There have been studies on the material response of composites subjected to a dynamic loading. Abrate has written a detailed review of literature on the

impact of laminated composites [2]. The review covers work from the late 1970s to early 1990s with a focus in discussing the experimental and theoretical approaches of early composites work. In the 2000s work by Zaretsky et al [3] and Yuan et al [4] focused on the damage of composite materials when subjected impact loading, specifically low velocity impacts. Current studies by Avachat and Zhou have experimentally and computationally modeled the dynamic failure of sandwich composites subjected to underwater impulsive loads. Their results yielded empirical solutions to optimize their structural design [5]. These studies, however, did not subject the composite specimens to aggressive marine environments prior to subjecting the composite material to dynamic loading.

Accelerated life testing (ALT) methods simulate long term exposure to marine environments and are used to study to the effects of exposure on mechanical properties of materials. In these investigations, composite materials are subjected to simulate marine aging through submersion in seawater baths at elevated temperatures [6-14]. Nakada and Miyano [15] have developed prediction methods for the long term fatigue life of fiber reinforced plastic (FRP) laminates under elevated temperature and absorption conditions. The long term effect of submersion on composite sandwich structures was studied by Siriruk et al [16] with focus on the interface between the face sheets and the core. Park et al [17] presented the effects of aging after an impact event on polymer composites in terms of residual properties. Submersion studies focus on the degradation of material properties due to the diffusion of water into the composite. Elevated temperatures are used to increase this rate of diffusion, therefore requiring

additional studies to determine the relationship between the exposure time in the accelerated life test and an equivalent time in a typical operating environment.

Diffusion studies to find an acceleration factor relating ALT submersion times to an equivalent time at operating temperatures have been conducted. These studies involve weight gain monitoring of samples to find diffusion coefficients [18]. Rice and Ramotowski [19] used the Arrhenius equation to derive a method for finding this acceleration factor using the matrix material of the composite. The factor was found to be dependent on the activation energy of the matrix, which is found experimentally.

Also, computational investigations of the mechanical response of composite materials have become more prevalent as accurate numerical models have become available. Simulations allow for a more cost effective way to test a variety of different variables affecting the mechanical response of a composite. The modeling of composite damage using finite elements has mainly been performed with strain rates up to those of drop weight testing. However, studies such as those of LeBlanc et al. [20] were able to correlate experimental results of the dynamic shock response of composite plates with finite element simulations using LS-DYNA. Arbaoui et al. [21] investigated modeling the response of composites in a split Hopkinson pressure bar (SHPB) experiment and were able to successfully correlate experimental data to their simulations. Material properties for the finite element simulations are taken from the results of quasi-static material testing, which has been proven to be accurate by Chan et al. [22].

In this study carbon/epoxy (CE) material will be subjected to quasi-static and dynamic experimentation before and after significant submergence in an elevated temperature, salt water solution. The results from the weathered and non-weathered experiments will be compared. Additionally, two computational models (0 and 30 day submergence) will be produced to simulate the dynamic experiment. Quasi-static behavior of the CE material will be used for generating the computational model.

Materials Studied

Composite

The composite material used in this investigation is a Carbon/Epoxy (CE) plate produced by Rock West Composites. The composite's fiber construction is a 2x2 twill weave cured in an epoxy resin. The plate is 2.92 mm thick and composed of a 670 GSM 12k carbon fiber fabric (Aksaca 12K A-42) and PT2712 low viscosity epoxy produced by PTW&W Industries, Inc. Fiber volume fraction of the material is ~60%. The total thickness of the CE panel is made up of four twill woven plies. The total composite plate mass per volume of the composite is 1.45 g/cm^3. An image of the composite material and the fiber construction is show in Figure 1.

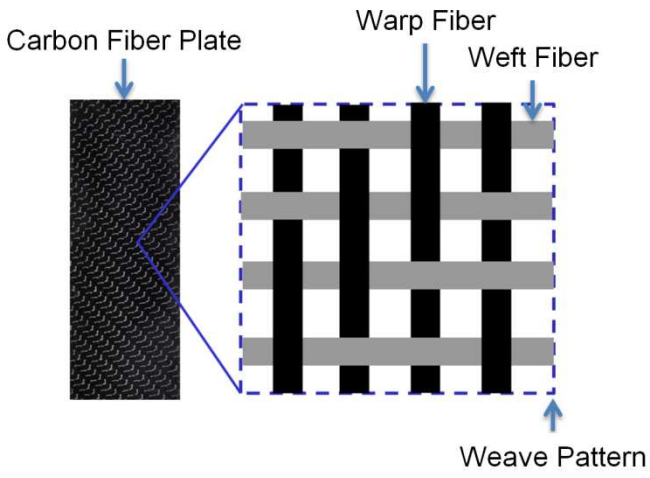

Figure 1: Zoomed representation of the 2x2 twill weave

Specimen Preparation

Specimens were prepared for a variety of testing methods with the 2.92 mm thick CE plate material. Panels of size, 0.305 m x 0.305 m were cut to specific dimensions with diamond saws. Diamond saws were utilized to avoid edge cracking

and delamination in the material. Two quasi-static tests and one dynamic experiment were performed requiring a variety of specimen dimensions. Table 1 displays the specimen dimensions for each experiment type. Note that all specimens were 2.92 mm in thickness. Dimensions are chosen to meet experimental specifications including ASTM standards D3039/D 3039M- 000 (tensile) and D7264/D7264M-07: Procedure B (four point bend) and prior studies (shock tube).

Table 1: Composite specimen dimensions by experiment type

Experiment Type	Tensile	Four Point	Shock tube
Dimensions (L cm x W cm)	25. 4 x 2.54	15.24 x 1.27	5.08 x 20.32

Prior to submergence testing, all specimens were desiccated for 48 hours to remove accumulated atmospheric moisture.

Experimental Setups and Methods

Submergence Tank

A submergence tank was created to subject CE panels to marine conditions. An image of the weathering setup is displayed in Figure 2. The tank is composed of two high temperature polypropylene reservoirs. A double wall is created by placing the volumetrically smaller tank inside the larger tank, creating a fluid boundary to separate the immersion heaters from the internal salt solution. The immersion heaters are separated to prevent any unwanted salt water corrosion.

A 35 ppt (3.5%) NaCl solution fills the internal tank and is where specimens are submerged for 30 and 60 days. The immersion heaters in the external tank are used to heat the external boundary of distilled water and through convection and

conduction, heat the internal salt solution. The tank is insulated with Styrofoam and maintained at a steady state of 65 ^{0}C. The temperature of 65^{0}C was chosen to increase the rate of aging in the composite material, while remaining below the published 71.7 - 95.6 °C glass transition temperature range of the epoxy resin from PTM&W Industries, Inc.

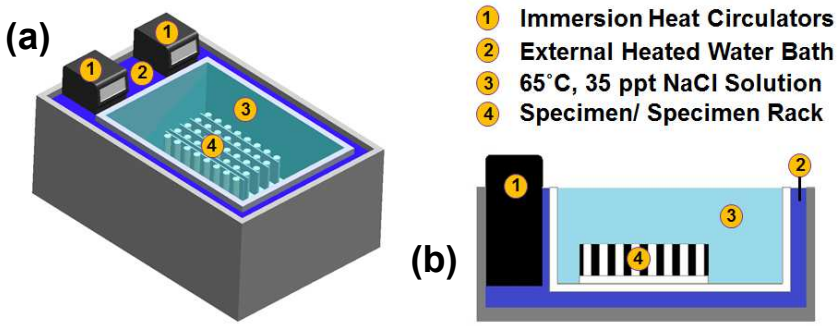

Figure 2: Submergence Tank (a) Isometric View (b) Cross Section Side View

The immersion heaters chosen to heat the submergence tank were Cole Parmer PolyScience LX Immersion Circulators. The maximum capacity of each heater is 20 liters of fluid with a temperature range of ambient to 98 ^{0}C. Temperature stability is ±0.07 ^{0}C.

Shock Tube

A shock tube apparatus is used to generate a concentrated in air shockwave that is imparted on the weathered and non-weathered composite panels. A schematic of the setup is shown in Figure 3.

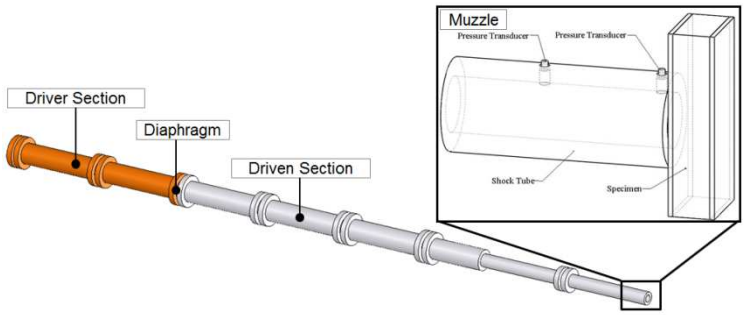

Figure 3: Shock Tube apparatus capable of creating a concentrated in air shockwave

The total length of the shock tube is 8 m and is composed of three separate sections: driver section, driven section, and reduced diameter muzzle. A Mylar diaphragm separates the driver and driven sections, while the driver section is pressurized using helium gas. Under critical pressure, the diaphragm bursts releasing a high pressure wave. The high pressure travels down the length of the driven section and develops into a shock wave front. The shockwave then travels through the muzzle section and the pressure of the event is captured by two dynamic pressure transducers. The pressure transducers capture the magnitude of the pressure while velocity of the wave can be inferred from the time between pressure histories and established positions of the sensors. Typical velocities range from Mach 1 to Mach 2. The shockwave then leaves the muzzle, impacts the specimen and the pressure from the impact is reflected back into the muzzle. The reflected pressure is the pressure that loads the specimen.

Digital Image Correlation (DIC)

2-Dimensional DIC

Time lapse photography coupled with 2D DIC is utilized to provide full field strain data during the tensile tests. This technique was employed to visually capture the non-uniform strain behavior of the composite material. Specimens were coated with spray paint to create a random speckle pattern (white background with black dots) which is used to track the deformation during quasi-static loading. A single camera angled perpendicular to the specimen tracks pixel subset intensities within a given resolution. Subsets are defined within the resolution thus defining a matrix of unique regions in the speckle. These regions are tracked over time and recognize changes in pixel intensities, in turn outputting deformations and full field in plane strain.

2D DIC methods are critical in composite deformation due to the anisotropic nature of the material and likely potential for localized areas of high deformation. Full field deformation allows for a more in-depth analysis of the quasi-static behavior of the CE composite.

3-Dimensional DIC

High speed photography coupled with 3D DIC is utilized to provide full field displacements, strain, and velocities of shock tube specimens during in air shock loading. Two cameras are used to track the out of plane displacement of the composite panels during a shock loading. Figure 4 shows that cameras are placed at a 7° angle, perpendicular to specimen and provide stereo vision to determine changes in 3 dimensional space. Similar to 2D DIC, pixel intensities are tracked within a given

resolution, however the utilization of two synchronized cameras provides 3D out of plane information.

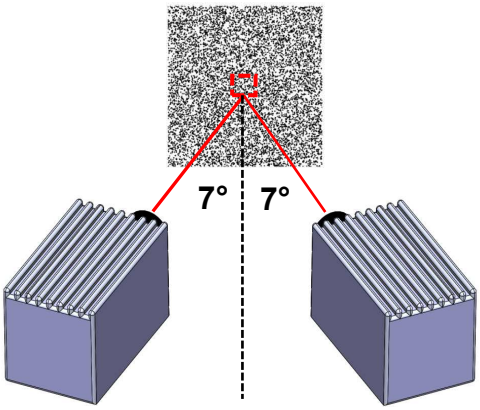

Figure 4: High speed camera setup viewing a speckle pattern in order to track 3D surface strains, displacements, and velocities

To record the transient response with the high speed system, the cameras must be calibrated and have synchronized image recording throughout event. The calibration of the cameras is performed by placing a grid containing a known pattern of points (dots) in the test space where the composite sample is located during the experiment. This grid is then translated and rotated in and out of plane while manually recording a series of images. This grid pattern is predetermined and the coordinates of the center of each point (dot) is extracted from every image thus allowing for a correlation of the coordinate system of each camera. Prior to conducting the experiments, the face of the composite plate facing the cameras is painted with a random speckle pattern (white background with small densely spaced black dots). The Photron Fastcam Viewer (PFV) software is employed to synchronize the high speed cameras and record the images during the experiments. PFV is a user interface that enables the editing and storage of captured images and

videos. The post processing is performed with the VIC-3D software package which matches common pixel subsets of the random speckle pattern between the deformed and un-deformed images. The matching of pixel subsets is used to calculate the three-dimensional location of distinct points on the face of the plate. This provides a full field displacement history of the transient event with time. The cameras used during experimentation were Photron FastCam SA1. Each camera is capable of frame rates from 1,000 to 675,000 fps with image resolution ranging from 1,024 x 1,024 to 64 x 16 pixels depending on the frame rate. In the current effort, a frame rate of 50,000 fps was utilized for an inter-frame time of 20μs.

Quasi Static Experimental Methods

Tensile Testing

Experiments performed establish the quasi-static properties of the composite material before and after accelerated environmental exposure. The ASTM tensile standard is followed to ensure proper specimen preparation, data collection and procedures (ASTM D3039/D 3039M- 000). Tensile quasi-static tests determined the ultimate tensile strength and tensile modulus of elasticity for each weathering scenario. Three batches of specimens with various amounts of weathering time are tested: 0 days, 30 days and 60 days. Specimens with 30 and 60 days were desiccated for 48 hours, submerged for the appropriate duration, removed after the submergence period, and then surface dried and tested the same day.

All samples were prepared with 3.81 cm long sandpaper grips bonded by JB Weld leaving 15.24 cm as the free length between grips. One side of the free length of the tensile specimens is speckled with black and white paint in order to perform 2D

DIC during experimentation. A CAD schematic of the test setup is displayed in Figure 5.

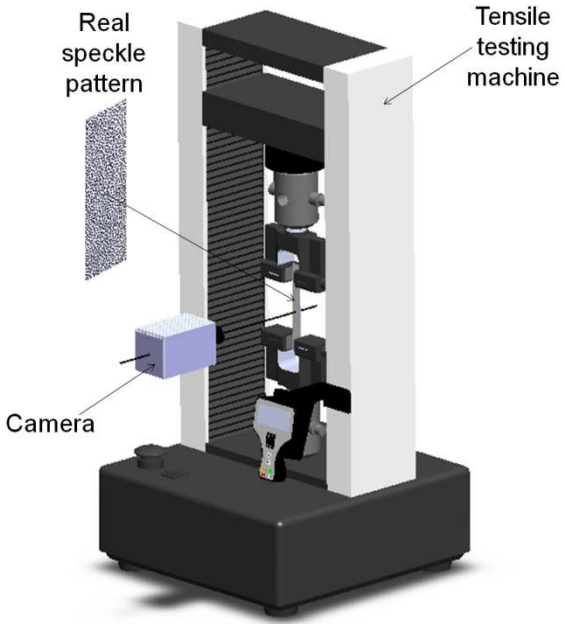

Figure 5: Instron testing machine equipped with a camera for 2D DIC

The sample is clamped in the Instron jaws on the sandpaper tabs. Prior to loading, a camera is placed perpendicular with additional lighting for time lapse photography. The sampling rate of the camera and the Instron is 1 Hz. The extension rate of the Instron is 2 mm/min to remain within ASTM standards.

Five experiments are conducted for each of the three weathering cases. The DIC images and Instron load cell are synced by manually triggering each system simultaneously. DIC in-plane strain data is combined with Instron loading data to create engineering stress vs. engineering strain curves. Both modulus of elasticity and ultimate tensile strength are determined for 0, 30 and 60 days.

Flexural Testing

Experiments performed establish the quasi-static properties of the composite material before and after significant weather exposure. ASTM flexural procedures are followed to ensure proper specimen preparation, data collection and procedures (ASTM D7264/D7264M- 07: Procedure B). Material properties sought by quasi-experimentation are ultimate flexural strength and flexural modulus. An image of the setup is in Figure 6.

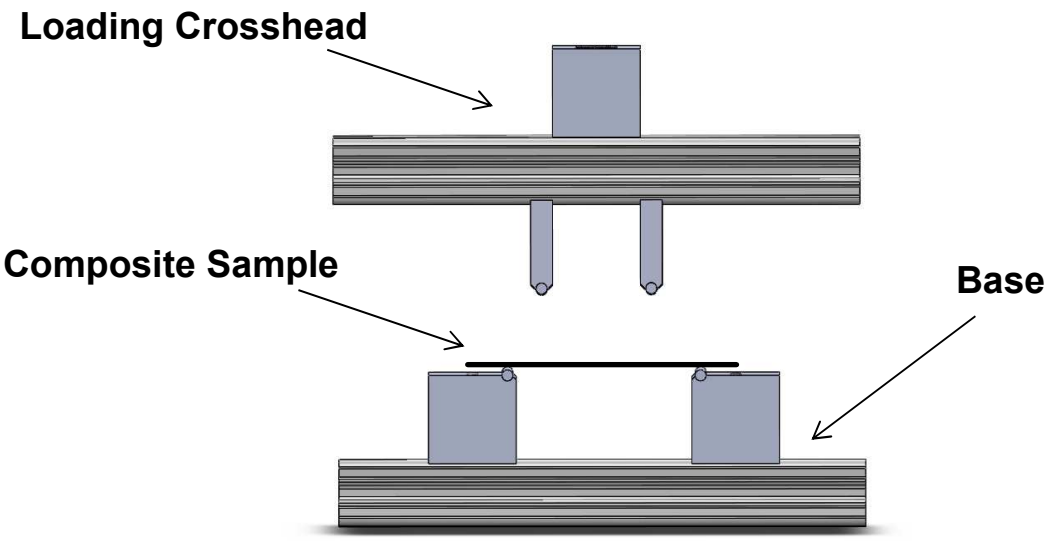

Figure 6: Four point bend setup

Dynamic Experimental Methods

Shock tube

Shock tube experiments are performed to establish the dynamic behavior of composite plates before and after prolonged submergence. Prior to experiments specimens were lightly sanded to create a rough surface so a speckle pattern could be applied. After speckling the composite, the plate is positioned vertically in the simple

support with a muzzle gap of (~0.1 mm). The specimen is oriented so the speckle pattern faces opposite the shock tube muzzle. Opposite the muzzle 3D DIC cameras are positioned to capture high speed images to monitor the deflection, strain and velocity of the plate during the dynamic shock event. A schematic of the experimental setup is shown in Figure 7.

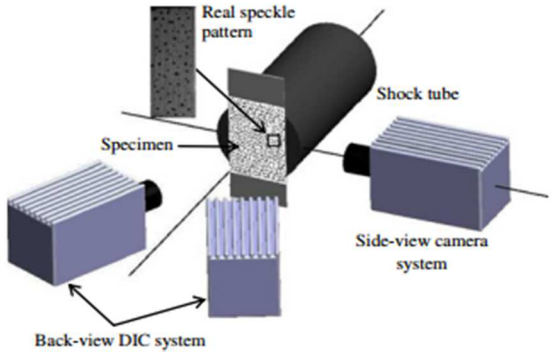

Figure 7: Shock tube setup displaying the high speed camera setup with respect to the muzzle

Two high speed cameras are setup to view the back face of the specimen for 3D DIC while a side view camera is positioned to view the out of plane deflection. Images of the event from all cameras are taken at 50,000 fps.

The pressure of the shockwave is created using a 0.127 mm thick Mylar diaphragm with a burst pressure of ~0.25 MPa. Two PCB Piezotronic, Inc. piezoelectric pressure transducers are mounted flush to the interior of the muzzle to measure shockwave pressures and velocity. Data is recorded using a Tektronix DPO 3034 Digital Phosphor Oscilloscope. The consistent burst pressure of the Mylar diaphragm and set muzzle standoff distance produce repeatable experiments. Three experiments for each weathering scenario are completed. Utilizing high speed 3D DIC full field dynamic behavior of the composite plates is obtained.

Weathering Acceleration Factor Methods

Arrhenius Relations and Theory

Degradation of material properties during aggressive marine exposure is highly dependent on a composite's matrix material. A dominant factor contributing to material degradation during prolonged submersion is fluid absorption in the matrix. Relating experimental weathering time (submergence time) to service time (in the field submergence time) in this study is accomplished by directly associating the rate of water absorption and time to total saturation of the matrix material, to a mathematical relation.

In order to mathematically relate the experimental submergence of the composite plate to real-life service submergence, a separate study of the matrix material is accomplished. The separate study assumes the only factor in the degradation of the composite's degradation is the damage to the matrix material via fluid absorption.

The mathematical relationship between the accelerated life test and real time immersion is governed by the Arrhenius equation (1). This equation describes the temperature dependence of the rate of reaction for a given process.

$$k = Ae^{\frac{-E_a}{RT}} \tag{1}$$

Where: k - Rate Constant

A - Prefactor

E_a - Activation Energy

R – Universal Gas Constant

T - Absolute Temperature

As mentioned, degradation of the material properties of composites from submergence is due to moisture absorption in the matrix material. A series of salt water solution soak studies is performed on the on the matrix material to determine diffusion coefficients and water saturation limits. The study is conducted at three temperatures: T_a, T_b and T_c degrees Celsius. The spread of diffusion coefficients at various temperatures produces Arrhenius activation energy for the matrix material, mathematically relating to an Acceleration Factor (AF). The AF will relate experimental temperature and time, to service (actual) time at various service temperatures.

Thin disks of the matrix material are produced to maximize the surface area for diffusion. Three disks are submerged in each temperature (T_a, T_b and T_c degrees Celsius) of the salt water solution in order to provide an average for each temperature case. Mass measurements of the disks are then recorded daily. All data collection ceases when all disk specimens have reached total saturation (mass equilibrium). Only until total saturation is t_{50}, the time required to reach 50% of the total saturation, known. Diffusion coefficients for each temperature are then be calculated using a reduced Crank's equation (2),

$$D = 0.049\frac{h^2}{t_{50}} \tag{2}$$

Where D is the diffusion coefficient and h is the thickness of the disk sample. Using the Arrhenius Equation and converting it into its logarithmic form, equation (3) is achieved:

$$\ln(D_T) = \ln(D_o) - \frac{E_a}{RT} \tag{3}$$

Where D_T is the diffusion coefficient at absolute (Kelvin) temperature T, D_o is a constant, E_a is the activation energy, and R is the universal gas constant. Plotting the $\ln(D_T)$ versus 1/T produces a linear slope. The slope is $-E_a/R$ and the absolute value are substituted into the function for AF.

$$AF = e^{\left(\frac{E_a}{R}\right)\left(\frac{T_2 - T_1}{T_1 T_2}\right)} \tag{4}$$

T_2 is the temperature in Kelvin that the accelerated testing is performed and T_1 is the theoretical service temperature the composite could experience in real-world conditions. By selecting the experimental and theoretical service temperature of the salt water solution, the AF can be calculated.

Diffusion Study Procedure

For the diffusion study, 3 beakers of 3.5% salt solution are prepared and maintained at different temperatures: 22, 45, and 65 °C. For each beaker temperature, 3 epoxy disks of PT2712, the epoxy in the carbon composite, are created. The disk dimensions are denoted in Figure 8. All 9 epoxy disks were desiccated for 48 hours to remove moisture and massed before submergence.

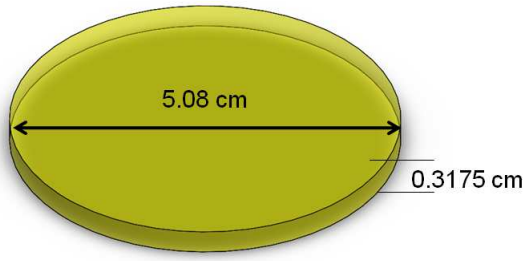

Figure 8: Diffusion study epoxy specimen labeled with dimensions

Three epoxy disks were submerged in each of the three beakers to ensure repeatability at each temperature. Figure 9 displays how the specimens were oriented to maximize the surface area exposed to the fluid. Throughout the duration of the experiment, epoxy disks were periodically removed from their beaker, dried, weighed, and placed back in their respective beaker. In the first 24 hours the specimens were weighed on average every 30 minutes with 3 minutes to mass specimens in each beaker.

As the rate of water diffusion into the matrix material decreased, the time between mass measurements of the specimens increased from 30 minutes to one week intervals. The percent mass increase was recorded for all epoxy disks and plotted versus time. Due to limited experimentation time, percent mass gain at saturation was obtained from the fastest beaker of epoxy disks to reach mass equilibrium. The two other beakers were continued to 50% total saturation. Total saturation was determined after specimens submerged in 65°C, 3.5% salt solution displayed no mass gain for more than 3 days. All epoxy disks eventually reach the same saturation, but at different rates.

Figure 9: Beaker setup with submerged epoxy specimen

Results and Discussion

Acceleration Factor

The percent weight gain in the epoxy specimens was measured for 60 days. Figure 10 shows the average percent mass increase for each temperature versus time. Since all specimens, independent of temperature, will reach the same saturation, the trials were ended at 60 days. Total saturation was obtained by the 65 °C samples and the remaining temperature trials reached at least 50% saturation, t_{50}, a value necessary to solve the Arrhenius solution. Figure 10, does not show all samples reaching total saturation since the trial was conducted for 60 days.

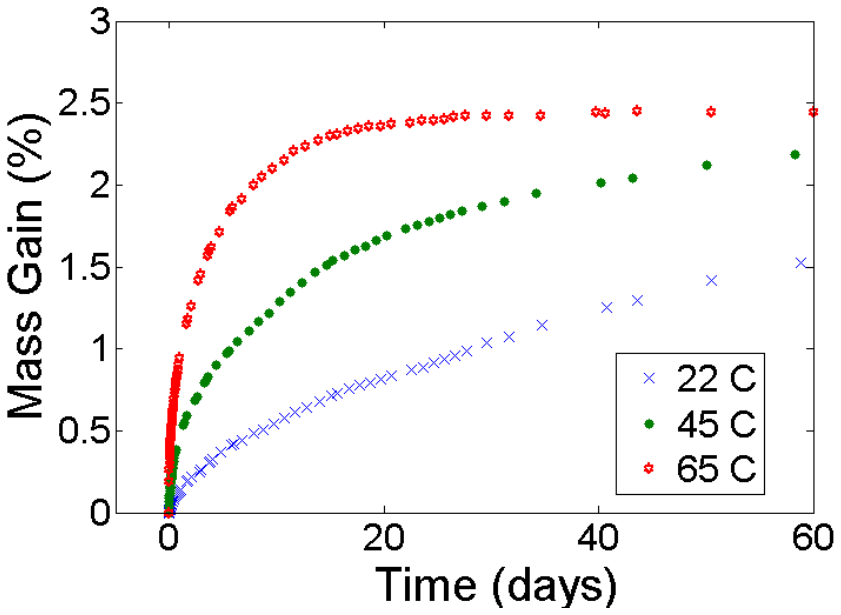

Figure 10: Average epoxy mass increase over time

Knowing t_{50} and the known thickness of the material, the diffusion coefficient D is calculated. In Figure 11 the natural log of D is plotted vs. 1/T and from the linear trend the activation energy is extracted.

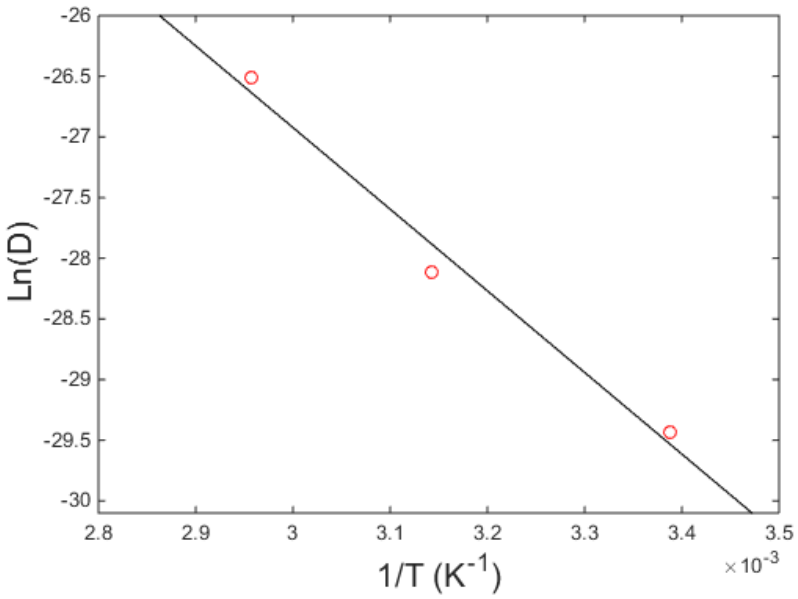

Figure 11: Natural logarithm of the diffusion coefficient versus each of the inverted three testing temperatures in Kelvin. The linear trend yields the activation energy of the epoxy.

The AF is then solved for, with the experimental submergence temperature (65 °C), and is displayed in Figure 12 (a) and Figure 12 (b). Figure 12 shows that with a decrease in service temperature the AF will increase.

From the diffusion study, the calculated acceleration factors range from 18 to 48, corresponding to service temperatures from 22 °C to 10 °C respectively. After 30 days of submergence, multiplying 30 days by the varying AFs, the real weathering time will be between 1.5 to 4 years of aging, dependent of service temperature. For 60 days, multiplying by the variation in AF, the aging range is between 3 and 8 years.

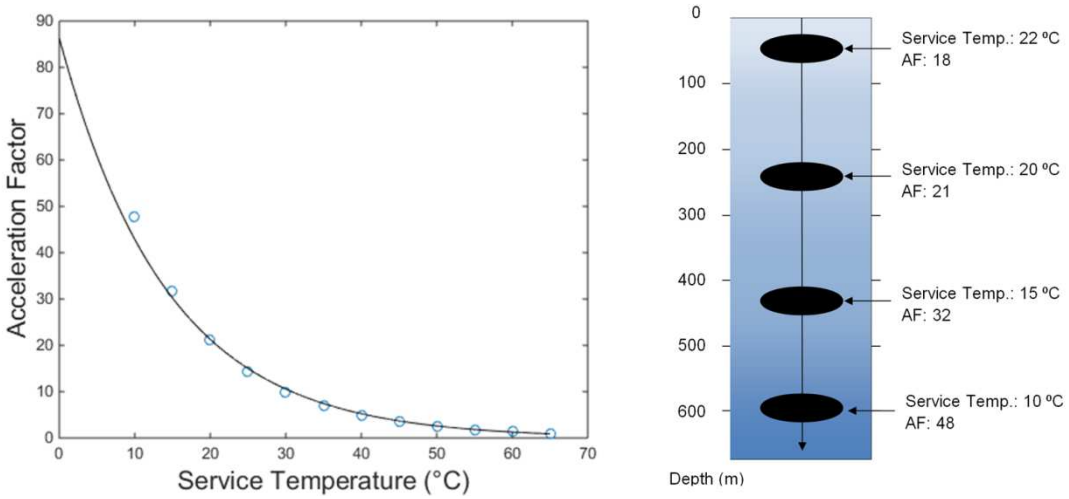

Figure 12: Acceleration factor (a) exponential variation of AF versus an increase in service temperature (b) visual representation of AF at various service depths

Quasi-Static Results

2D DIC was employed to view the full field, non-uniform, tensile strain. This behavior is depicted in Figure 13. 2D DIC proved to be highly beneficial in locating regions of high strain, displaying strain patterns, and pinpointing areas of failure.

In Figure 13 the strain field shows diagonal regions of higher strain. The diagonal pattern of the composite is formed from the 2x2 twill weave of the carbon fiber. This localized strain behavior is determined to be non-load bearing carbon fiber tows oriented perpendicular to the loading direction. While the carbon fibers oriented in the loading direction beard the load, the fibers perpendicular to the loading direction were not utilized in tension. This behavior led to the load distributing primarily into the matrix material producing locations of higher strain in turn leading to cracking in the matrix material. Failure of the composite is brittle and catastrophic.

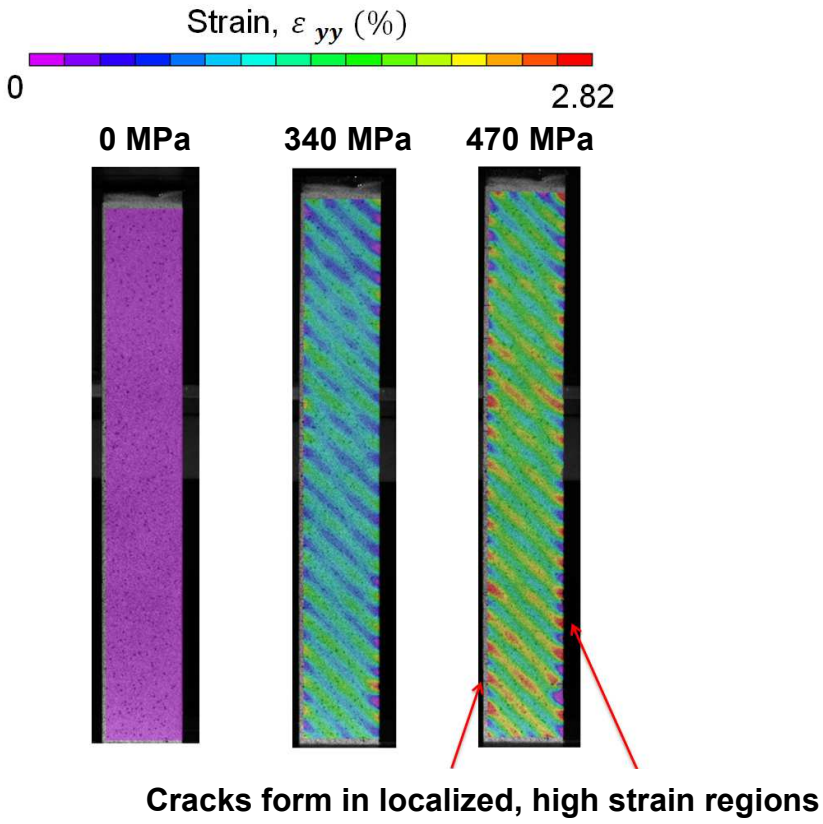

Figure 13: Full field strain for tensile experiments

The average quasi-static behavior of the material before and after salt water submergence is listed in Table 2. In order to determine a tensile modulus for the composite material, an average was taken from the total correlated area. The tensile modulus takes into account the global composite properties; however there are areas of high, localized strain. Table 3 displays the percent change in the average mechanical properties of the 30 and 60 day cases. For all cases, a minimum of five experiments were performed.

Table 2: Quasi-static properties after various submergence times

Exposure Time (Days)	Tensile Modulus (GPa)	Ultimate Tensile Strength (MPa)	Ultimate Flexural Strength (MPa)
0	53 ± 8.8%	563 ± 7.4%	554 ± 6.2%
30	47 ± 4.1%	496 ± 5.9%	433 ± 10%
60	47 ± 5.2%	492 ± 4.1%	424 ± 4.2%

Table 3: Variation (% change) in quasi-static behavior after various submergence times

Exposure Time (Days)	Tensile Modulus	Ultimate Tensile Strength	Ultimate Flexural Strength
30	-11%	-12%	- 22%
60	-11%	-13%	- 23%

After 30 and 60 days of submergence the mechanical behavior of the composite material decreased respectively: tensile modulus decreases by 11% and 11%, the ultimate tensile strength by 12% and 13% and flexural strength by 22% and 23%. After 60 days of submergence, the properties show to have degraded within 1% of data accrued from 30 days of exposure.

Dynamic Results

Due to similarities in experimental results for the 30 day and 60 day submergence, both quasi-static (tensile and four point) and dynamic (shock tube), only the 0 day and 30 day weathering experiments are discussed in the following results. The averaged quantitative results for the quasi-static and dynamic behavior are within 2%.

Shock tube

Experiments were performed with a dynamic shock pressure of ~0.8 MPa for all experiments. A minimum of three experiments were performed for each scenario to ensure repeatability.

Figure 14 is a plot of the dynamic pressure created by the shock tube apparatus versus time in milliseconds. Two distinct regions in the profile are labeled. The Incident Pressure, is the decayed pressure created by the shock tube when the Mylar diaphragm ruptures. The Reflected Peak Pressure is a product of the Incident Pressure and the interaction with the composite plate at the end of the shock tube. This reflected peak is ultimately the pressure in which the plate is being loaded. Once the reflected peak pressure is reached, the pressure will decay to ambient pressure over time. Figure 14 is an example of the experimental pressure attained by the pressure sensor closest to the specimen in two different experiments. The plot is representative of good pressure agreement between the experiments.

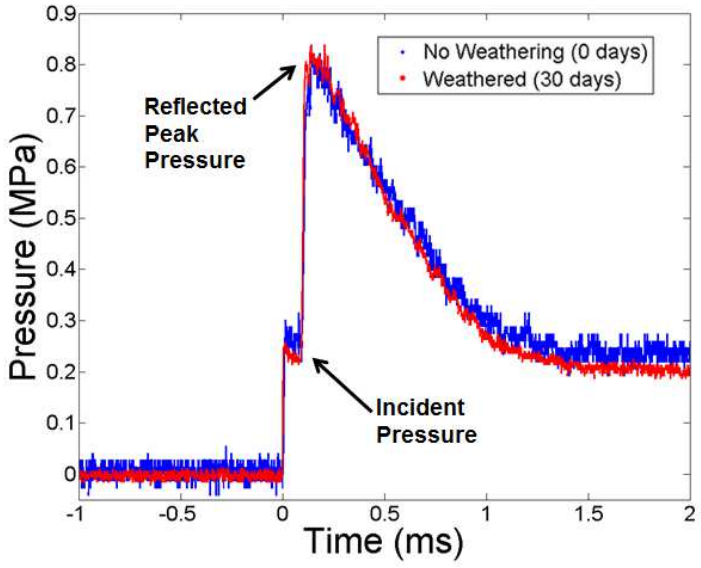

Figure 14: Typical shock tube pressure profiles

Side View Images

Figure 15 is a series of images from each weathering scenario captured throughout the dynamic blast loading event. Throughout times 0 to 0.8 ms the behavior of the composite material displays similar out of plane deflection. The 0 day weathered specimen deforms, in what appears to be elastic deformation (internal damage cannot be accounted for) and returns to its original form. However, at time 1.2 ms, the 30 day weathered specimen displays cracking in the compression region, and in the subsequent frames, a crack develop through the composite panel thickness. The crack leads to a complete break through the thickness of the composite.

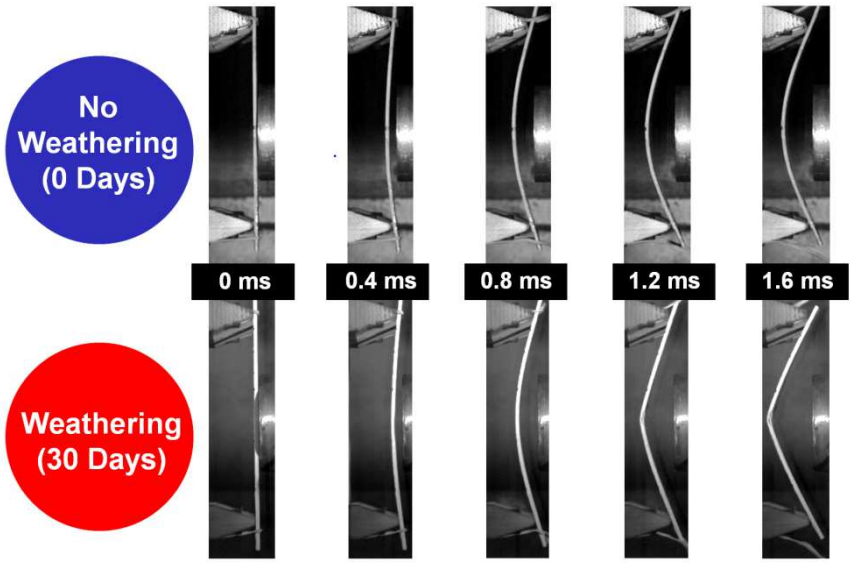

Figure 15: Side view images of the composite plate during the shock loading event

3D DIC and Maximum Deflection

Cracking behavior is confirmed in the 3D DIC data. Images plotted in Figure 16 display the full field out of plane deflection on the same scale from 0 to 40 mm.

Similar to the side view images, the composite panels from each case have similar out of plane deflections until 1.2 ms. From times 1.2 to 1.8 ms the 30 day case shows greater deflections originating at the center of the panels where the initial load is applied. At 1.8 ms the 3D DIC de-correlates in the region of highest deflection due to through thickness cracking. In all experiments performed at 30 and 60 days the composite panels catastrophically failed by through laminate cracking.

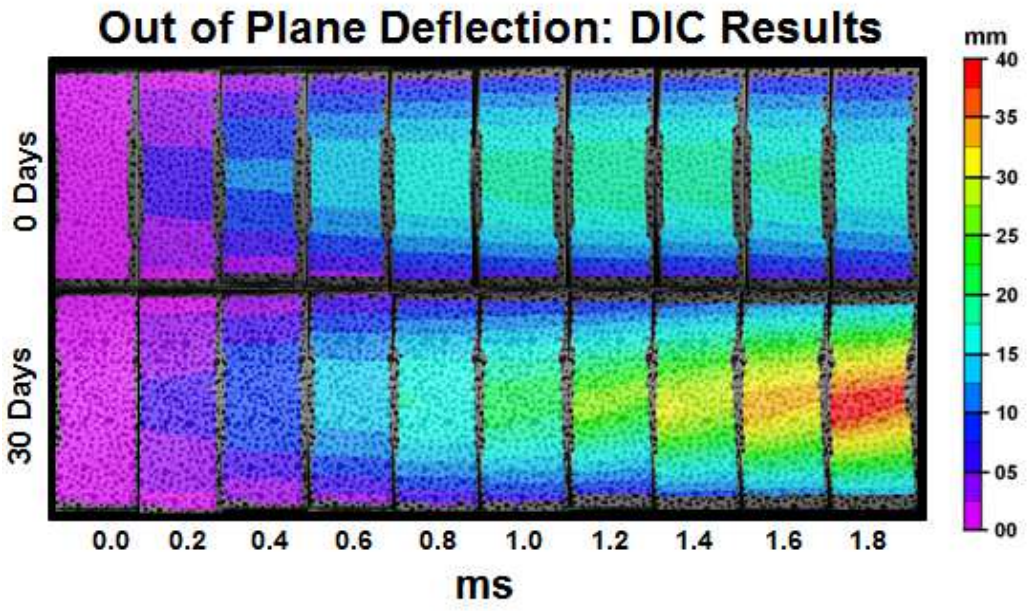

Figure 16: Full field out of plane deflection throughout the shock loading event

Using the full field 3D DIC data, the maximum out of plane deflection is plotted for each weathering scenario in Figure 17. Observed cracking of the 30 day, weathered composite is determined to be at 1 ms from images captured by the side view camera. From the center point deflection versus time the rate of deformation

remains consistent between all experiments, but the load bearing capacity significantly decreases, as an effect of weathering, leading to brittle catastrophic failure.

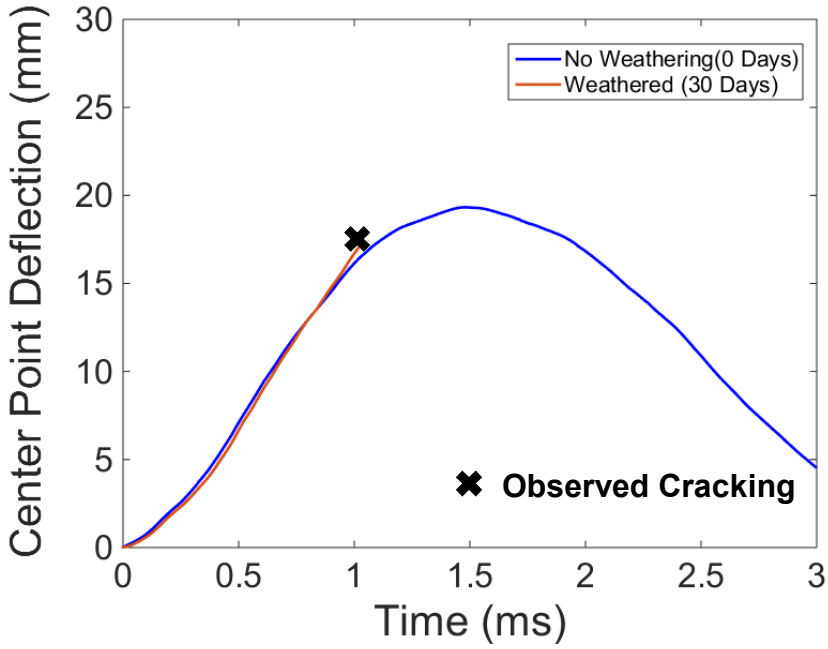

Figure 17: Maximum Back-face Center Point deflection extracted from the 3D DIC data

Post Mortem and Damage Mechanisms

Utilizing the information obtained from the high speed images and post mortem material, strong conclusions can be made as to how the material failed and how weathering, as diffusion plays a role in degrading the mechanical properties.

After 0 days of weathering, the composite panel deflects significantly after the dynamic blast load, but remains structurally elastic. Figure 18 shows an image of the panel after loading showing no external brittle or plastic behavior occurred. The

composite proved to be extremely resilient in maintaining its structure; however conclusions cannot be made about internal damage such as matrix fiber de-bonding or fiber breakage. In order to determine internal damage a technique such as ultrasonic scanning must be employed.

After 30 and 60 days of weathering the damage mechanisms leading to catastrophic failure showed distinct similarities. From the side view images, a crack is seen developing from the compression region of deflection, further propagating through the composite thickness. Commonly, continuous fiber composites do not behave well in compression because the tensile strength of the fiber is not utilized. This behavior typically leads to localized buckling of the material while in compression. After significant time in submergence, the matrix material's mechanical properties inevitably deteriorated leading to failure in compression. This failure, therefore, compromised the structure leading to crack propagation in the composite laminate. Images of the fractured 30 day submerged composite can be seen in Figure 18. A post mortem image of the 60 day specimen is not shown as the failure was both transiently and physically identical to 30 days of submergence. The fibers in the post mortem images are short in nature meaning brittle, catastrophic failure occurred through fiber fracture rather than fiber pullout.

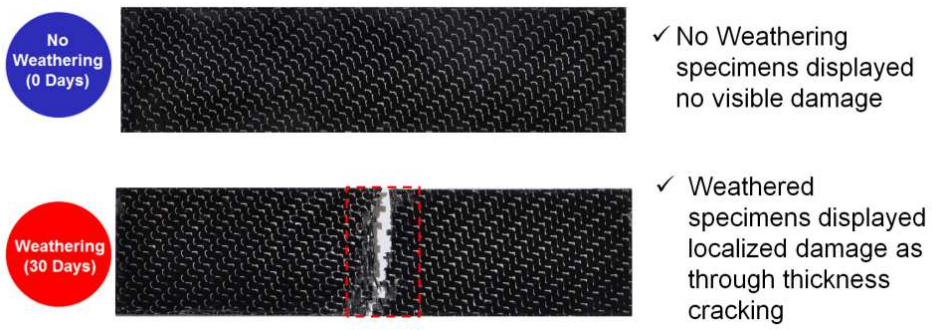

Figure 18: Post mortem images of shock tube specimens

Additional quantitative evidence of matrix initiated and matrix dominant failure is apparent in the DIC, in-plane strain data. The maximum strain achieved prior to through fracture in all weathered experiments is between 1.6-1.8%. The failure strain of the carbon fiber is 1.8% meaning while the damage occurs during the dynamic shock loading, the carbon fibers have not reached their failure limit. Damage occurring during the dynamic load can then be considered to be matrix dominated.

Finite Element Modeling

Finite element modeling (FEM) for the shock loading experiments was performed using the LS-DYNA code available from the Livermore Software Technology Corporation. Two models were created for the 0 day and 30 day weathering scenarios.

The 19.7 x 5.08 x 0.292 cm composite plate is modeled with solid elements and consists of 4 element layers through the 0.292 cm thickness. Each layer represents one of the 4, 2x2 twill woven plies in the plate. A 4% frequency damping (100-600 Hz) is applied to the computational model.

The material model used in the numerical simulation is the Mat_Composite_Failure_*Option*_Model (Mat_059, Option = Solid). This model

allows for mechanical failure in tension, compression or shear. Mechanical properties determined from the quasi-static experimentation were used to create the model. Although mechanical properties are known to change with respect to the rate of loading, the quasi-static properties for each weathering scenario were sufficient to conduct the numerical study. Steel support pins were implemented in addition to the composite model to create a realistic, simply supported boundary condition. A complete image of the FEM model is displayed in Figure 19 (a).

Shock loading was applied to the surface of the composite plate by introducing an experimental pressure profile into the computer model. The shock imparted on the front face of the specimens was created to be realistically non-uniform; distributed in decreasing steps of magnitude as a function of increased radius. The 3.81 cm diameter muzzle region is assumed to be uniform, however due to plate deformation and pressure spreading as a function of time, the pressure distributed radially outside the muzzle diameter is decreased linearly (in steps) in magnitude with respect to radius as shown in Figure 19 (b). A similar computational approach is documented in the Composite Structures journal titled, Experimental and numerical study of foam filled corrugated core steel sandwich structures subjected to blast loading by Yazici et al.

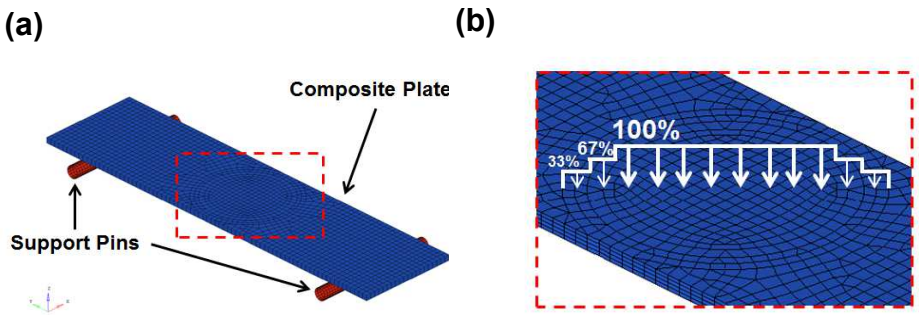

Figure 19: (a) Fully meshed composite plate model with boundary condition support pins (b) Circularly meshed loading area displaying the step loading applied

Full Field Results

From the FEM model, the full field behavior of the transient event can be visualized. In Figure 20, each weathering scenario's computational transient behavior is plotted with their corresponding experiment. Figure 20 displays the full field out of plane displacement for the first 1.8 ms of the dynamic shock event for each weathering scenario, 0 and 30 days of submergence. From the visual results, the simulation appears to be in excellent agreement with experimental data.

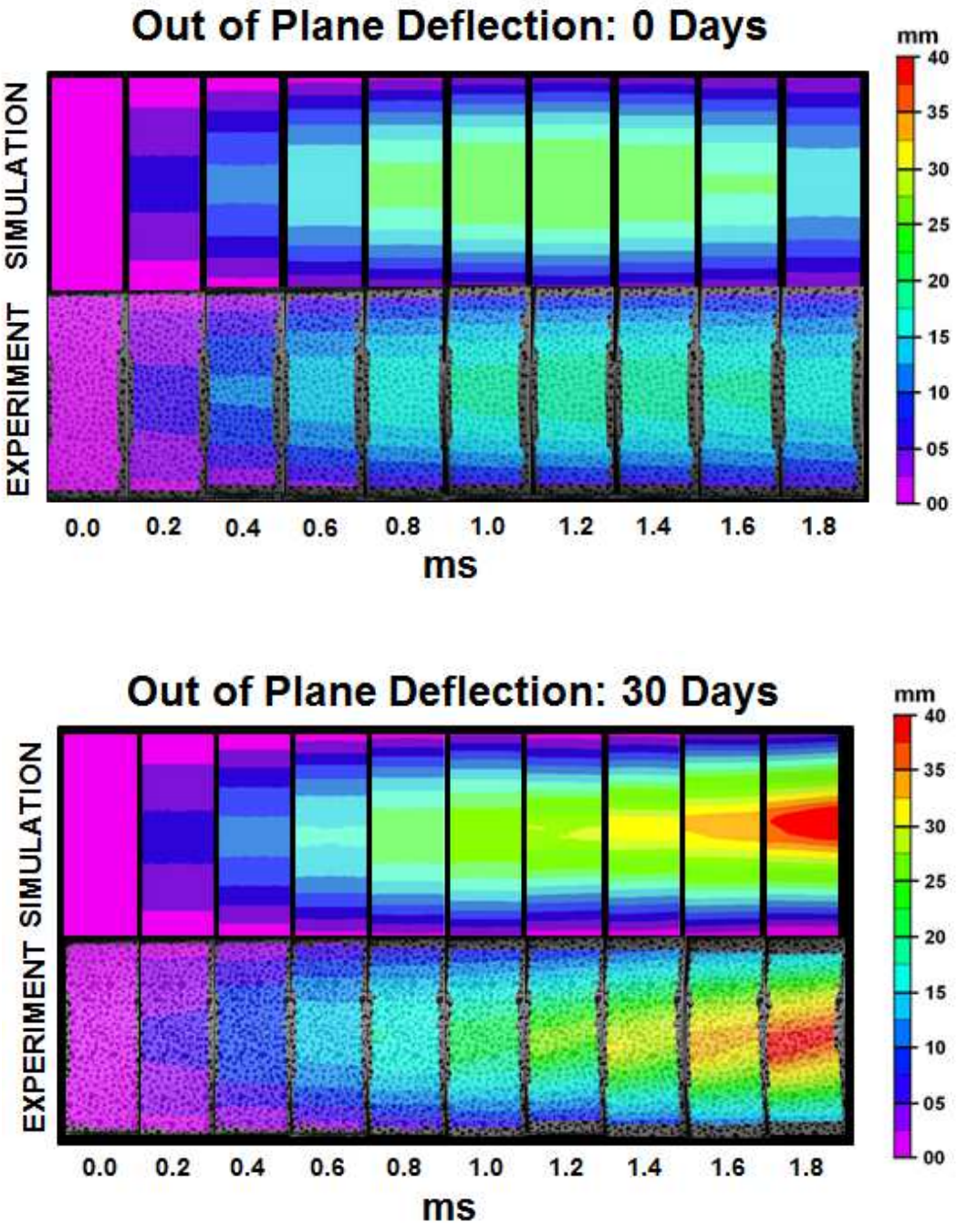

Figure 20: Full Field Simulation and Experimental Visualization

Computational Correlation to Experimental Results

To ensure accurate results between experiments and the simulation, the level of correlation must be quantified. The center point deflection time history of the model is

extracted from the simualtion and experimental images to provided quatifiable data. The technique used to correlate this data is known as Russell Error [23]. Russell Error compares transient data by quantifying the variation between magnitude and phase of data sets. Both types of error are then condensed into a comprehensive error measurement. The relations for these error measurements are listed below:

$$RP = \frac{1}{\pi}\cos^{-1}\left(\frac{\sum c_i m_i}{\sqrt{\sum {c_i}^2 \sum {m_i}^2}}\right) \qquad \textbf{\textit{phase}}$$

$$RM = \text{sign}(m)\log_{10}(1 + |m|) \qquad \textbf{\textit{magnitude}}$$

$$RC = \sqrt{\frac{\pi}{4}(RM^2 + RP^2)} \qquad \textbf{\textit{comprehensive}}$$

In the equations above c_i and m_i stand for the simulated and experimental (measured) response values, respectively. The quality of correlation is categorized by RC value as follows:

RC ≤ 0.15	***excellent***
0.15 < RC ≤ 0.28	***acceptable***
RC > 0.28	***poor***

Figure 21 shows the extracted center point experimental data for each weathering scenario with their corresponding simulation. From the Russell error relations in Table 4 and the corresponding relation listed below the comparison plots, it is determined the simulation and experimental data agreement is excellent.

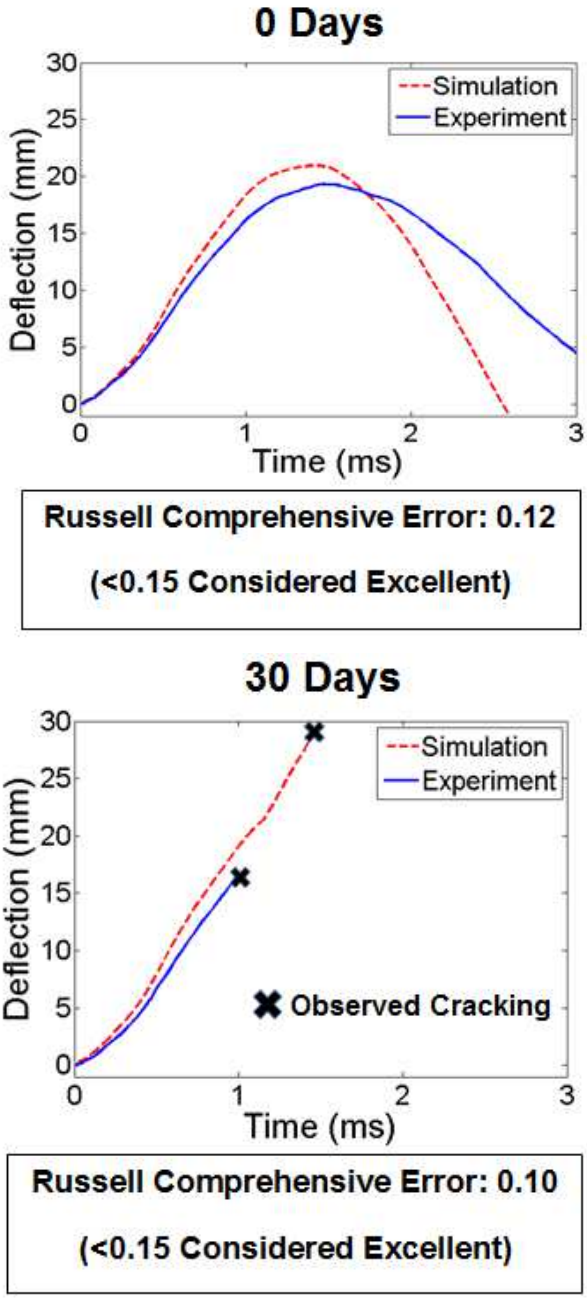

Figure 21: Deflection plots of experimental and computational modeling

Table 4: Russell Error summary

	Center Point Delfection	
	0 days	30 days
Phase Error (PM)	0.13	0.01
Magnitude Error (RM)	- 0.02	- 0.11
Corresponding Error (CM)	0.12	0.10

Conclusions

Based upon experiments performed to study effects of prolonged submersion, it was concluded after significant salt water exposure, the mechanical properties of carbon/epoxy composite degrades. The summary of the results are as follows:

- The diffusion study showed that the AF for the composite material ranged from 18 to 48. This corresponds to a range of service temperatures from 22 °C to 10 °C. The actual aging time of the composite ranges from 1.5 to 4 years for 30 days of submergence and 3 to 8 years for 60 days of submergence.
- After 30 days of exposure, the quasi-static mechanical properties decreased significantly. Specifically, the tensile modulus and tensile strength decreased by 12% and 28% respectively.
- After 60 days of submergence the quasi-static mechanical properties of the composite essentially did not change from the properties at 30 days submergence.

- Shock loading experiments displayed vastly different behavior with respect to 0 day versus 30 and 60 day exposures.
    - The non-weathered (0 day) composite panels displayed maximum out of plane deflection on average of ~20 mm. After multiple oscillations the panels, in all experiments, elastically returned to their original form. Internal damage was not accounted for in these experiments; however there was likely internal damage such as fiber breakage and matrix cracking.
    - Early in the shock loading, the 30 and 60 day panels showed similar deflection versus time, but catastrophically failed before reaching 20 mm. The panels displayed cracking on the compression face of the panel that propagated throughout the thickness of the material.
    - It can be concluded that brittle-like failure occurred throughout the dynamic event since the region of failure there was visible evidence of short fibers, thus implying fiber fracture rather than fiber pullout.
- Computational models in LS-DYNA showed excellent correlation with experimental data

Acknowledgements

The authors acknowledge the financial support provided by the Naval Engineering Education Consortium (NEEC) Grant # 3003266434 and the financial

support of the Naval Undersea Warfare Center (Division Newport) Chief Technology Office.

References

[1] Mouritz, A.P., Gellert, E., Burchill, P., Challis, K. “Review of Advanced Composite Structures for Naval Ships and Submarines”, Composite Structures 53.1 (2001) 21-42.

[2] Abrate, Serge. "Impact on Laminated Composite Materials." Applied Mechanics Reviews Appl. Mech. Rev. 44.4 (1991): 155-90.

[3] Zaretsky, E., deBotton, G., Perl, M. “The Response of a Glass Fibers Reinforced Epoxy Composite to an Impact Loading”, International Journal of Solids and Structures 41 (2004) 569–584.

[4] Yuan, F.,Tsai, L., Prakash, V., Rajendran, A.M., Dandeka, D., “Spall Strength of Glass Fiber Reinforced Polymer Composites”, International Journal of Solids and Structures 44 (2007) 7731–7747.

[5] Avachat, Siddharth, and Min Zhou. "High-speed Digital Imaging and Computational Modeling of Dynamic Failure in Composite Structures Subjected to Underwater Impulsive Loads." International Journal of Impact Engineering 77 (2015): 147-65.

[6] Xu, L. Roy, Arun Krishnan, Haibin Ning, and Uday Vaidya. "A Seawater Tank Approach to Evaluate the Dynamic Failure and Durability of E-glass/vinyl Ester Marine Composites." Composites Part B: Engineering43.5 (2012): 2480-486.

[7] Kootsookos, A., and A.p. Mouritz. "Seawater Durability of Glass- and Carbon-polymer Composites." Composites Science and Technology64.10-11 (2004): 1503-511.

[8] Li, Xiaoming, and Y.jack Weitsman. "Sea-water Effects on Foam-cored Composite Sandwich Lay-ups." Composites Part B: Engineering 35.6-8 (2004): 451-59.

[9] Sala, G. "Composite Degradation Due to Fluid Absorption." Composites Part B: Engineering 31.5 (2000): 357-73.

[10] Weitsman, Y. Jack. "Effects of Fluids on Polymeric Composites—A Review."Comprehensive Composite Materials (2000): 369-401.

[11] Dewimille, B., J. Thoris, R. Mailfert, and A.r. Bunsell. "Hydrothermal Aging Of An Unidirectional Glass-Fibre Epoxy Composite During Water Immersion." Advances in Composite Materials (1980): 597-612.

[12] Aveston, J., A. Kelly, and J.m. Sillwood. "Long Term Strength Of Glass Reinforced Plastics In Wet Environments." Advances in Composite Materials (1980): 556-68.

[13] Jain, R.k., and K.k. Asthana. "Effect Of Natural Weathering On The Creep Behaviour Of Grp Laminates In Tropical Climates." Advances in Composite Materials (1980): 613-23.

[14] Jain, R.k., S.k. Goswamy, and K.k. Asthana. "A Study of the Effect of Natural Weathering on the Creep Behaviour of Glass Fibre-reinforced Polyester Laminates." Composites 10.1 (1979): 39-43.

[15] Nakada, M., Miyano, Y., “Accelerated Testing for Long-Term Fatigue Strength of Various FRP Laminates for Marine Use”, Composits Science and Technology 69 (2009) 805-813.

[16] Siriruk, A., Penumadu, D., Weitsman, Y. J., “Effect of Sea Environment on Interfacial Delamination Behavior of polymeric Sandwich Structures”, Composites Science and Technology 69 (2009) 821-828.

[17] Park, S.W., Veazie, D.R., Zhou, M., “Post-Impact Aging of FRP Composite Laminates in the Marine Environment”, Proceedings of the 14th Engineering Mechanics Conference, Austin, TX, May 2000.

[18] Augl, J., Berger E., (1976). *The Effect of Moisture on Carbon Fiber Reinforced Epoxy Composites| Diffusion*. Naval Surface Weapons Center: Silver Spring,MD.

[19] Rice, Matthew, and Thomas, Ramotowski. "Activation Energy Calculations for the Diffusion of Water into PR-1590 and Pellethane 2103-80AE Polyurethanes." (2011)

[20] LeBlanc, James, and Arun Shukla. "Dynamic Response and Damage Evolution in Composite Materials Subjected." *Composite Structures* 92.10 (2010): 2421-430.

[21] Arbaoui, Jamal, Mostapha Tarfaoui, and Aboulghit EL Malki. "Mechanical Behavior and Damage Kinetics of Woven E-glass/Vinylester Laminate Composites

under High Strain Rate Dynamic Compressive Loading: Experimental and Numerical Investigation." *International Journal of Impact Engineering* (2015): n. pag. Web.

[22] Chan S, Fawaz Z, Behdinan K, Amid R. “Ballistic limit prediction using a numerical model with progressive damage capability.” *Composite Structures* (2007): 77: 466–74.

[23] Russell DM. “Error measures for comparing transient data, Part I: Development of a comprehensive error measure, Part II: Error measures case study.” *Proceedings of the 68th Shock and Vibration Symposium* (1997).

CHAPTER 2

NEARFIELD UNDERWATER EXPLOSION RESPONSE OF POLYUREA COATED COMPOSITES

by

James LeBlanc, Christopher Shillings, Erin Gauch, Frank Livolsi, Arun Shukla

Published in Experimental Mechanics

Corresponding Author: James LeBlanc

Naval Undersea Warfare Center

Newport, Rhode Island 02840

Structural, Materials and Mechanical Engineer

Phone: 401 – 832 – 7920

Email: James.M.LeBlanc@navy.mil

Abstract

An experimental study is conducted to evaluate the response of polyurea coated E-Glass / Epoxy composite plates subjected to near field underwater explosion (UNDEX) loading with an air backed boundary condition. Experiments are performed in a water filled blast tank in which the transient plate response during the UNDEX loading is measured. The response is measured using a technique called Digital Image Correlation and is implemented with high speed photography. Images of the plate are captured during the UNDEX event and are processed to provide full field displacements, strains and velocities of the structural response.

Three geometries are tested: a 0.762 mm thick composite plate (control), a 1.524 mm thick composite plate and a 1.524 mm thick plate half composite, half polyurea coating. The experimental results show that the transient response of the control plate is improved in reducing out of plane deflection in two ways: by utilizing a thicker composite plate or through the application of a polyurea coating. However adjusting the deflection response with respect to an areal weight ratio (AWR) shows the polyurea coating is the best in reducing deflection with respect to the structure's total relative weight.

Additionally, the polyurea coating plays a critical role in reducing damage accrued by the plate during the UNDEX event. In experiments without a polyurea coating, the composite plates shear at the fully clamped boundaries, thus leading to water penetration into the air backed region. The composite coated with polyurea resists shearing and maintains the boundary between the water and air.

Introduction

An interest of the United States Navy is to construct new vehicles and structures from composite materials. The advantages of using composites include: high strength to weight ratios, lighter structural components, and overall reduced maintenance costs. However, when structures manufactured from these materials are employed in military applications they must also be designed to survive underwater explosions (UNDEX). The static response of composite materials is well understood while there is less of an understanding when composites are subjected to dynamic load conditions like an UNDEX. This gap in knowledge typically leads to an overdesign of composite structures where the advantages of using a composite are not fully utilized.

When an explosive is detonated at a large standoff distance from a structure, the shock front is nearly planar and acts uniformly over the entire structure. The structure reacts with globalized deflections. Under this loading condition there tends to be less material damage (primarily inter-laminar delamination) and the susceptibility of plate ruptures decreases. Since the plate typically does not rupture, the shock wave is almost fully reflected after contact with the structure, shielding any occupants and/or internal equipment from the effects of dynamic, high pressure. Conversely, when an explosion occurs directly on, or very close to, the surface of a structure, the loading area is concentrated. The result is highly localized pressure loadings and the structure sustains higher amounts of damage, oftentimes including plate penetration or complete rupture. When rupture occurs the high pressure fluid can enter the structure and damage to the panel may become shrapnel.

Studies on composite materials subjected to high loading rates have been studied with both experimental and computational techniques. Work by Latourte et al [1] utilized a scaled fluid structure method [2] to study the failure modes and damage mechanisms in both monolithic and sandwich plates subjected to underwater impulsive loads. Schiffer and Tagarelli [3] have compared the response of glass and carbon reinforced composites and found that the glass reinforced plates had larger blast resistance than the carbon plates due to their higher tensile ductility. Avachat and Zhou [4] studied the effects of underwater shock loading on filament wound and sandwich composite cylinder and found that while both constructions exhibited similar damage mechanisms, including delamination, fiber failure and matrix cracking, the sandwich structure had overall better performance than a monolithic cylinder with similar mass. The same authors [5] also utilized an Underwater Shock Loading Simulator combined with digital image correlation to show that for sandwich constructions lower density cores yield higher blast performance than high density cores due to their larger core compression capability. LeBlanc and Shukla [6, 7] have studied the response of flat and curved composite plates to far field underwater explosive loading through experimental and computational methods. Franz et al. [8] and Mouritz et al. [9] studied the effects of an underwater explosion at different standoff distances on a glass composite laminate. Dear and Brown [10] have conducted a detailed study on the damage mechanisms and energy absorption in composite plates when subjected to impact loading.

In recent years, the use of polyurea materials to enhance the failure resistance of structures subjected to explosive loading has become a topic of interest. Polyurea is

a synthetic, high strength, high elongation coating that is typically spray cast onto existing structures to increase their performance under shock and ballistic loading events. The armed forces have begun investigating the suitability of these materials for use on military and naval vehicles such as Humvees, troop carriers and ship hulls, Hodge [11]. Research efforts have recently studied the effectiveness of polyurea when used with composite materials. LeBlanc et al. [12, 13] showed that the transient response of UNDEX loaded composite plates is dependent upon coating thickness and coating location. Tekalur et al [14] investigated the response of E-Glass composites coated with polyurea subjected to air blast loading. This study indicated that the polyurea coating reduced the transient deflections and post mortem damage levels as compared to the uncoated material. Gardner et al [15] studied the effect of location of the polyurea in relation to the foam core in sandwich composites. It was observed that when a layer of polyurea is placed between the foam core and the back-face of the sandwich the blast resistance is improved, while conversely if the polyurea is placed between the front face and the foam core, the performance is reduced. Furthermore, effects of polyurea coatings have been studied with computational simulations. Amirkhizi et al [16] have developed a visco-elastic constitutive material model that describes the behavior of polyurea materials under a broad range of strain rates, and includes pressure and temperature effects. Amini et al [17, 18] used LS-DYNA to simulate impact and impulsive loading experiments of polyurea coated steel plates.

Material and Specimens

In the current study, E-Glass Epoxy bi-axial laminate composite plates, with and without polyurea coatings are studied. The following section details the materials utilized in the investigation.

Composite

The composite material used in this investigation is Cyply® 1002, a reinforced plastic manufactured by Cytec Engineered Materials. The material is a cured epoxy composite which contains a non-woven, parallel fiber construction of continuous E-Glass filaments. The layup of the composite is a cross-ply construction with alternating plies of 0° and 90°. Each ply has a thickness of 0.254 mm (0.01 in.). The cured material has an areal weight of 0.46 kg/m^2 (0.85 lb/yd^2) per 0.254 mm thick ply and a specific gravity of 1.85. The fiber volume fraction is 64 ± 3%. Two plate thicknesses, 0.762 mm and 1.524 mm are studied. The 0.762 mm plate is a 3 lamina construction, [0/90/0], and the 1.524 mm plate is a 6 lamina construction, [0/90/0/90/0/90]. The properties for a single unidirectional ply of the material are provided in Table 1.

Table 1: Cyply 1002 - Mechanical Properties (Uni-Directional)

	MPa
Tensile Modulus (0°)	39.3e3
Tensile Modulus (90°)	9.65e3
Tensile Strength (0°)	965
Tensile Strength (90°)	20
Compressive Strength (0°)	883
Compressive Strength (90°)	193

Polyurea

In the current work three geometries of plates are studied: the 0.762 mm composite plate (control), a 1.524 mm thick composite plate and a 0.762 mm composite plate coated with a 0.762 mm polyurea coating. The final geometry results in a plate with a combined thickness of 1.524 mm, equal to that of the thicker composite plate, later to be compared. The polyurea is spray coated to the back side of the plate after manufacturing. The construction is chosen to represent what would typically be found in a real world application where structures are retrofitted with a spray coating rather than fully integrated into the original design. After coating the composite it is post cured for 48 hours at a temperature of 71°C.

The polyurea material used is Dragonshield-BC available from Specialty Products, Inc. of Lakewood, WA. It's a 2 part material that can be spray cast to a wide range of surfaces and materials. The polyurea is characterized in both tension and compression for strain rates from 0.01 s^{-1} to 2000 s^{-1}. Characterization up to 100 s^{-1} was performed using standard material testing machine whereas a split Hopkinson pressure bar was used to characterize the response of the material at 2000 s^{-1}. The response of the material at 2000 s^{-1} is only characterized in compression and is assumed to be similar in tension. At the lower strain rates unique tests were conducted for both tension and compression. The full material characterization is shown in Figure 1. From this figure it is seen that the material exhibits strong strain rate dependence and becomes stiffer with increasing loading rate. Furthermore the

material displays a stiffening effect in compression above 30% whereas in tension the response exhibits a stress plateau like behavior.

A summary of the plate thicknesses and areal weights is provided in Table 2, and a schematic of the three laminate geometries tested are shown in Figure 2.

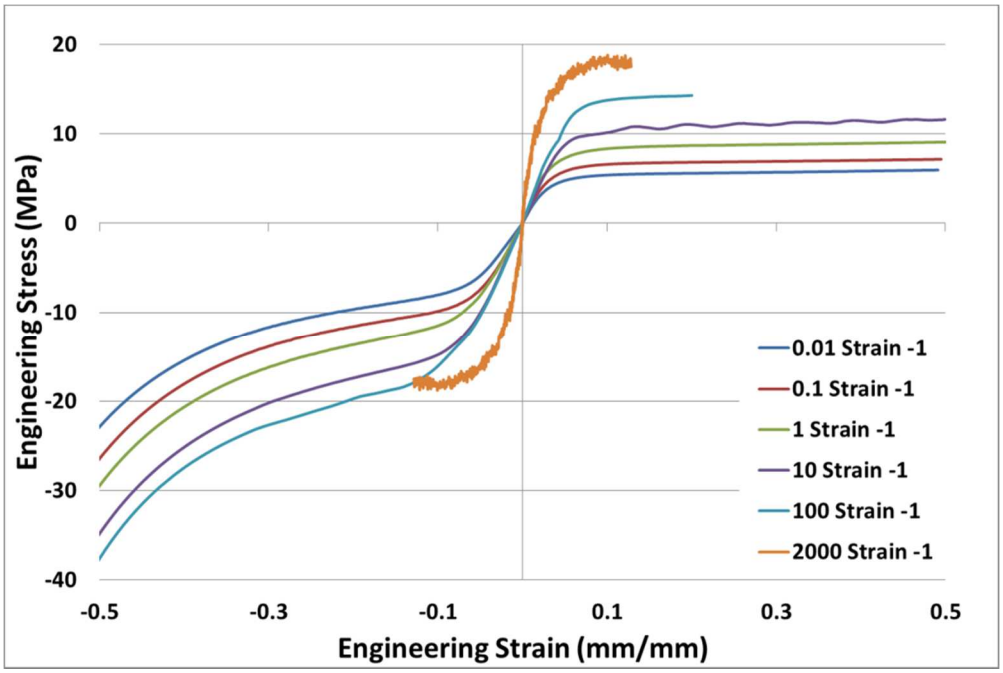

Figure 1: Dragon Shield BC Polyurea Stress-Strain Behavior

Table 2: Thickness and Areal Weight of Laminates

	Thickness, mm (in)	**Areal Weight, kg/m^2 (oz/yd^2)**
Thin Baseline Laminate	0.762 (0.03)	1.45 (42.7)
Thick Baseline Laminate	1.524 (0.06)	2.91 (85.5)
Thin Baseline with Polyurea coating	1.524 (0.06)	2.28 (67.4)

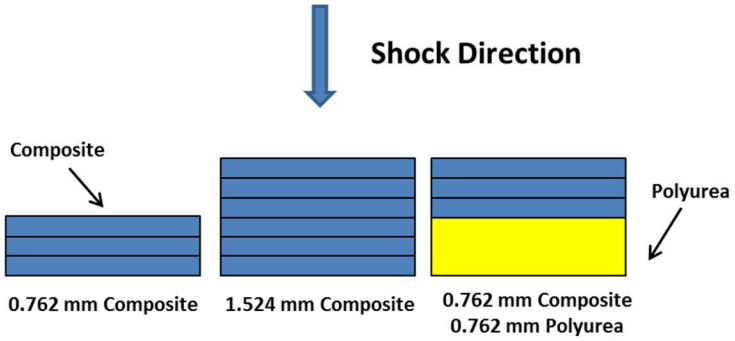

Figure 2: Composite Plate Construction – Schematic (Not to Scale)

Experimental Methods

Experiments conducted in this study utilize a water filled tank integrated with high speed photography to view the composite panel, with and without a polyurea coating, after the detonation of a near-field UNDEX. High speed photography is coupled with a technique called Digital Image Correlation to extract full field displacements, strains and velocities during the transient event. The following are the details of the equipment and methods employed.

Test Tank

The near field UNDEX experiments in this study are conducted in a water filled tank, Figure 3. The tank has internal dimensions of 1.21 m x 1.21 m x 1.21 m with 6.35 mm thick steel walls and is supported on a reinforced wooden stand. The tank contains ~1500 liters of water when filled. Four window ports allow for the lighting and high speed photography of the UNDEX event and plate motion. Mounted to the inner surface of one wall is a 304.8 mm x 304.8 mm, rectangular tunnel with a wall thickness of 12.7 mm, which serves as the base for the mounting of the composite

plates. The tunnel extends 394 mm into the tank from the wall and a 38.1 mm wide flange is welded to the end of the tunnel. The outer dimensions of the flange are 381 mm x 381 mm. The flange has a series of through holes around the perimeter which allow for bolting of the test plates to the flange. The test plates are sandwiched between the flange and a removable steel frame and are secured to the flange with a series of 1.59 mm diameter through bolts spaced at 38.1 mm. The use of the tunnel and mounting flange provide a water tight seal around the test plate and allows for the plates to be air backed, Figure 3. The composite plate and mounting fixture geometrical details are provided in Figure 4.

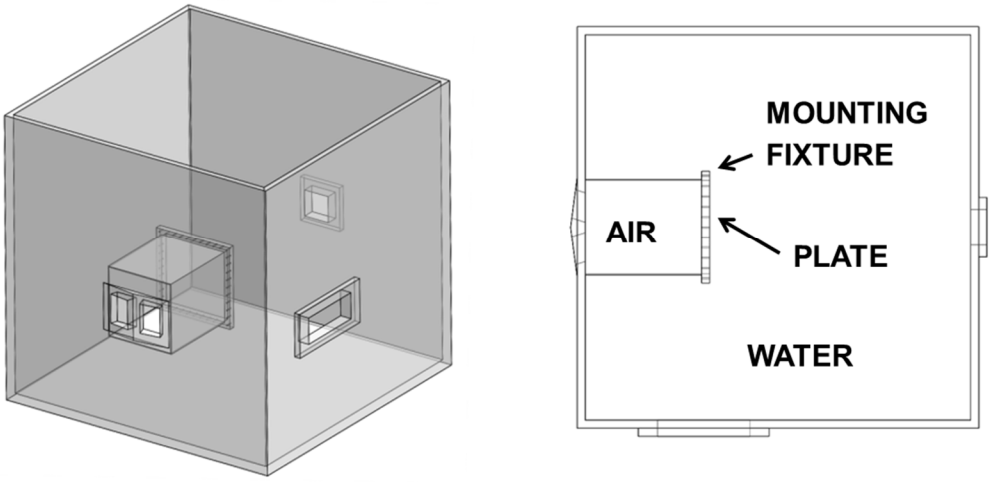

Figure 3: UNDEX Test Tank

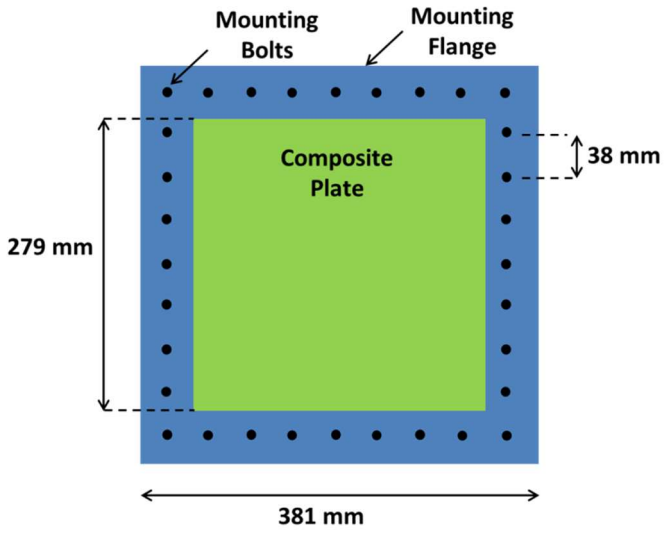

Figure 4: Specimen Geometry

Explosive Charge

The explosive used in the near field blast experiments is an RP-503 charge manufactured by Teledyne RISI, Figure 5. The charge is composed of 454 mg RDX and 167 mg PETN contained within an outer plastic sleeve. The charge strength is equivalent to that of 1 gram of TNT.

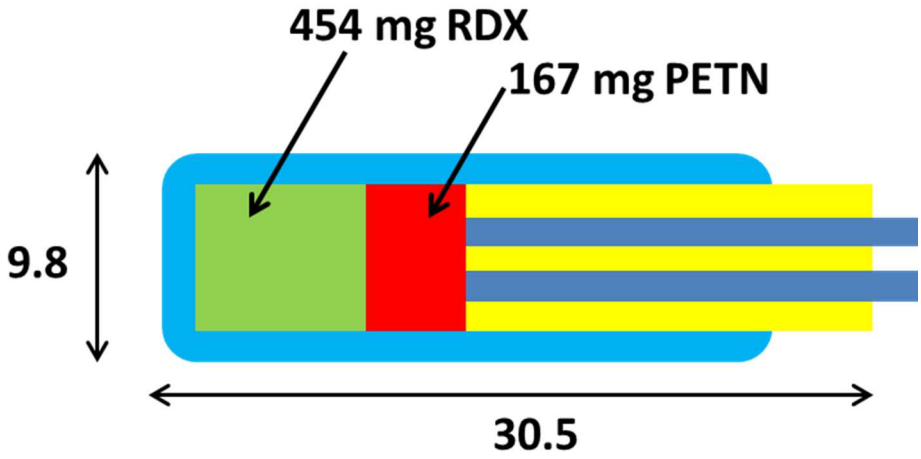

Figure 5: RP-503 Explosive Charge (units of mm)

Measurement Equipment

Pressure Transducers / Data Recorder

The pressure transducers used to measure the pressure field after the detonation of the RP-503 charge are Series 138 ICP Tourmaline Underwater Blast Sensors produced by PCB Piezotronics, Inc. (Item number 138A05). The sensors have a pressure range of 34.475 MPa, rise time less than 1.5 μs, and a resonant frequency greater than 1MHz.

A Tektronix DPO 3034 Digital Phosphor Oscilloscope is used to record the pressure histories during the near field blast experiments. The oscilloscope has 4 analog channels, each with a 2.5 GS/s sample rate, 300 MHz bandwidth, and 5 mega-point record length.

Digital Image Correlation

High speed photography, coupled with three dimensional Digital Image Correlation (DIC) is used to capture the full-field deformation of the back-face (side opposite of the explosive) of the plate during the UNDEX loading. During the experiments two cameras are arranged in a stereo configuration in order to view the back face of the test specimen. To record the transient response of a dynamically loaded plate, the cameras must be calibrated and have synchronized image recording throughout the event. The calibration of the cameras is performed by placing a grid containing a known pattern of points (dots) in the test space where the composite sample is located during the experiment. This grid is then translated and rotated in and out of plane while manually capturing a series of images. Since the geometry of

the grid pattern is known, the coordinates of the center of each point (dot) is extracted from every image thus allowing for a correlation of the coordinate system of each camera. Prior to the conduct of the experiments, the face of the composite plate facing the cameras (back-face) is painted with a random speckle pattern (white background with small densely spaced black dots).

The software employed to synchronize the high speed cameras and record the images during the experiments is Photron Fastcam Viewer (PFV). PFV is a user interface that enables the editing and storage of captured images and video. The post processing is performed with the VIC-3D software package that takes the series of captured video images, and tracks common pixel subsections of the random speckle pattern between the deformed and un-deformed images. The matching of pixel subsections is used to calculate the three-dimensional motion of distinct points on the face of the plate. This provides a full-field displacement history of the transient event throughout time.

The cameras used during experimentation were Photron FastCam SA1. Each camera is capable of frame rates ranging from 1,000 to 675,000 fps with image resolution ranging from 1,024 x 1,024 to 64 x 16 pixels respectively. In the current effort, a frame rate of 27,000 fps was utilized for an inter-frame time of 37μs. The camera resolution for the experiment is 448 x 480 pixels.

Experimental Methodology

Experiments are preformed to understand the behavior of E-Glass/Epoxy plates subjected to near field underwater explosions. Three plate configurations are studied: (1) 0.762 mm thick uncoated plate (control), (2) 1.524 mm thick uncoated plate, and

(3) 0.762 mm thick plate with 0.762 mm polyurea coating on the back-face. Two high speed cameras are positioned 330 mm behind the tank walls perpendicular to the viewing windows to avoid any distortion effects from the windows themselves. A third high speed camera is positioned at the side of the tank to view the detonation of the explosive, resulting bubble growth, and interaction of the bubble with the composite plate. Two free field tourmaline pressure sensors are located within the tank to record the pressure field at two distinct standoff distances. Let it be noted that the gages are located at a larger standoff from the charge than the distance between the charge and the composite plate to avoid damage to the sensors. Figure 6 is a combination, isometric view and aerial schematic of the tank providing an overview of the camera, explosive and pressure sensor positioning. An overview of the experimental process is presented in the following discussion.

To begin the experiment, the high speed cameras are calibrated to establish a virtual coordinate systems. Calibration is conducted according to the previously described method in which images of a calibration grid are captured while rotating and translating the grid. Once acceptable calibration and time syncing of the cameras is established the plate is bolted into the fixture with the black and white speckle pattern facing the cameras (air backed side). When mounting the polyurea coated plates, the coating is located on the back side of the composite plates, opposite of the charge location. Once the plate is bolted into the fixture the RP-503 charge is placed within the tank. The charge is suspended by its detonation wire into the tank and placed 50.8 mm from the center of the composite plate. To ensure consistent charge standoff distances for each experiment a 3.18 mm diameter foam spacer is placed between the

charge and plate. The foam is secured to both the charge and plate by a fast setting epoxy. The use of this foam spacer is critical to the conduct of the experiments for two reasons: (1) it ensures there is no variation of the charge location during the filling of the tank, and (2) it accounts for panel flexure (induced the hydrostatic load of the water after filling) by ensuring that the charge moves with the plate, thus maintaining a consistent standoff distance. Two tourmaline pressure sensors are positioned in the tank at horizontal standoff distances from the charge center of approximately 100 and 175 mm. The sensors are suspended in the tank from their water resistant cables and are secured to a weight on the bottom of the tank by means of a thin line to maintain relative positioning. Each sensor is then fixed in position by a wire which is secured to a weight resting on the bottom of the tank. After the plate is secured in the fixture and the pressure sensors are in place, the tank is filled with water to a depth of 1.06 m. The center of the plate is located 0.55 m below the surface of the water.

Once the tank is filled, and the operation of all measurement equipment is verified, the RP-503 charge is detonated with a detonation box. The box simultaneously sends a high voltage to the RP-503 charge to initiate detonation and a simultaneous 9 volt pulse to the oscilloscope to trigger the recording of UNDEX pressure history. The oscilloscope also relays a negative TTL voltage to each camera to capture the high speed photos. The use of this single initiation system is setup to synchronize the charge detonation and trigger the oscilloscope/cameras. Upon completion of the experiment all images from the DIC cameras are processed through VIC 3D to extract full-field plate deformation.

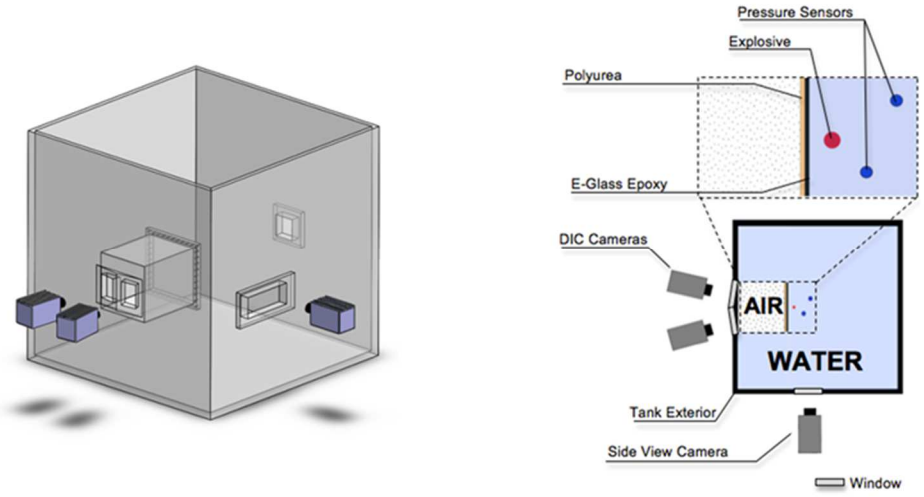

Figure 6: Experimental Setup Measurement Equipment

Results and Discussion

The response of the composite plates in this study is characterized by the transient center-point displacement of the back-face of the plate, deformation evolution mechanisms during the displacement, and full-field DIC observations. All plate deflection data presented for the plates is extracted from the post processed images through DIC.

The pressure profiles resulting from the detonation of the RP-503 charge, as measured by the two free field pressure sensors at 100 and 175 mm standoff distances from the charge, are shown in Figure 7. The pressure profiles display the characteristic components of an UNDEX, namely: a rapid pressure increase associated with the shock front, followed by an exponential decay and a reduction in peak pressure with increasing radial standoff from the charge center. It is noted that for the 100 mm standoff pressure gage there is a sudden drop in pressure occurring at 0.12 ms. This corresponds to the arrival of the reflected pressure wave from the surface of the plate. The peak pressure of the shock front experienced by the plate surface (50.8

mm standoff) is on the order of 40 MPa determined from the computational simulations.

The behavior of the bubble resulting from the detonation and its associated interaction with the composite plate is shown in Figure 8. The sequence of images shows the clear formation of the bubble at 80μs and its subsequent growth in size due to the combustion of the explosive products. Due to the high pressure of these gaseous products the bubble expands, reaching a diameter of ~50 mm at 320 μs at which point it reaches and interacts with the surface of the composite plate. As a result of this interaction with the plate its growth is arrested in the direction of the plate, but continues a spherical expansion in the remaining directions. The uncoated plates experience edge tearing (see later discussion) between 1200 μs and 1400 μs during which time the bubble is still expanding and has not yet reached its maximum diameter. Once tearing of the plate occurs, the plate can no longer be considered a standing plate and any resulting bubble behavior would be heavily influenced the global motion of the structure. Figure 8 displays only the first 560 μs of the bubble behavior to show initial plate contact and radial expansion. Times between 560 and 1200 μs consist mainly of further bubble expansion, thus images after 560 μs are not shown.

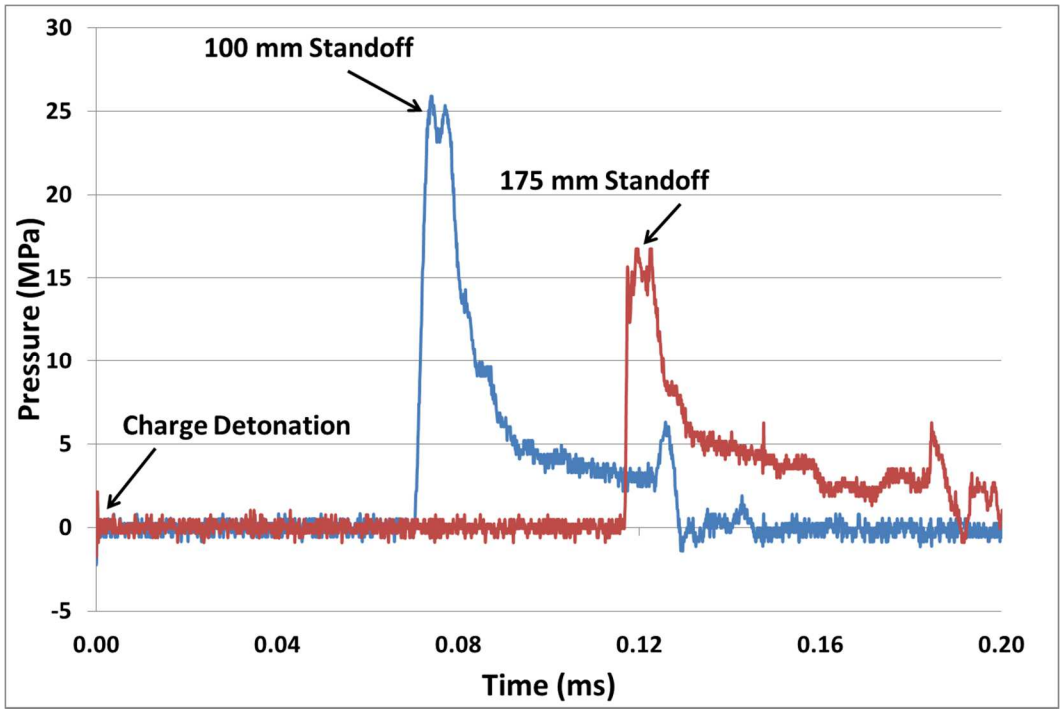

Figure 7: UNDEX Pressure Profiles (Time zero corresponds to charge detonation)

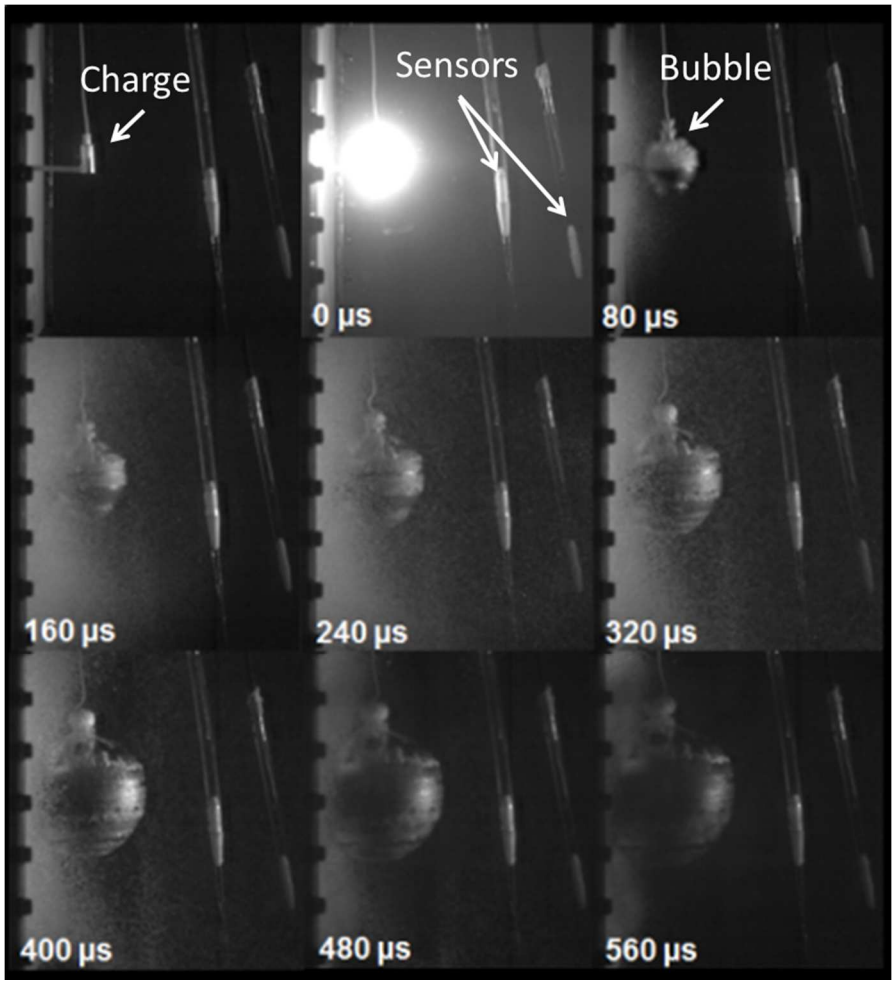

Figure 8: UNDEX gas bubble behavior

While filing tank with water during the setup of the experiment, it was observed that the plates sustain a measurable level of flexure due to hydrostatic pressure. The average peak center-point deflection of the plates after filling the tank is provided in Table 3. These deflections are determined by taking photographs of the plate surface before and after filling the tank and processing the images through the DIC software. The baseline for all subsequent plate deflection measurements is taken to be the deformed shape after tank filling. As previously described, a constant charge standoff for all plate configurations is achieved through the use of a foam spacer. Although beyond the scope of the current study, it is noted that it is likely that as the

initial depth pressure is increased (i.e. a deep diving submersible) the effects of the corresponding pre-stress prior to UNDEX loading should be considered. As the material has a finite strength capability, the additive effect of depth pressure and UNDEX pressure loading will reduce the ability of a structure to resist an explosion event that may have been survivable at shallower depths.

Table 3: Specimen deflections under hydrostatic preload

Plate	Deflection (mm)
0.762 mm	5.6
0.762 mm (Coated)	5.3
1.524 mm	4.6

The center-point displacement for each respective plate configuration is shown in Figure 9. From this figure it is observed that there are several distinct differences in the overall plate response as influenced by the plate construction. The first difference is the overall center-point deflection of the plates. It is evident that, as compared to the baseline 0.762 mm plate, increasing the plate thickness or including a polyurea coating reduces the peak overall deflection for a given level of loading. The peak displacement for the uncoated 0.762 mm plate is 28 mm, whereas for the 1.524 mm uncoated plate and the 0.762 mm polyurea coated plate the peak deflections are 20.5 mm and 24.8 mm, reductions of 27% and 12% respectively. It is noted that the center-point velocity during the initial deflection is nearly constant for each configuration. The main difference is the time that it takes for the plate to arrest its outward motion and begin to recover, with the 1.524 mm uncoated and the 0.762 mm polyurea coated plates arresting their outward motion ~0.25 ms sooner than the baseline 0.762 mm

plate. The peak center-point deflection and time to reach the peak displacement are provided in Table 4. The center-point deflection comparison between the 1.524 mm uncoated plate and the 0.762 mm plate with a 0.762 mm coating of polyurea indicate that for a plate thickness it is more advantageous to utilize additional structural plies rather than an elastomeric coating. However, when a structure has previously been designed and further thickening of the structural shape is not possible, the application of a polyurea coating can improve the transient response to shock loading.

The second primary difference in the response of the plate configurations is the onset of material damage. Both the uncoated 0.762 mm and 1.524 mm specimens experienced significant through-thickness tearing at the plate boundaries at approximately 1.1 and 1.4 ms respectively. Upon rupture of the plate edges water entered the cameras' field of view and caused de-correlation in the DIC images. Their plots, Figure 9, are accordingly abbreviated at the onset of tearing prior to DIC de-correlation due to water intrusion. However, it is further observed that although the 0.762 mm plate with the polyurea coating did experience larger deflections than the 1.524 mm uncoated plate, there was no edge tearing of the plate itself. Thus in terms of reducing material damage itself, the polyurea coatings offer an advantage over a thicker uncoated plate.

Table 4: Plate center-point deflection results

Plate	Maximum Deflection	Time to Peak
0.762 mm	28.2 mm	1.07 msec
0.762 mm (Coated)	24.8 mm	0.78 msec
1.524 mm	20.5 mm	0.74 msec

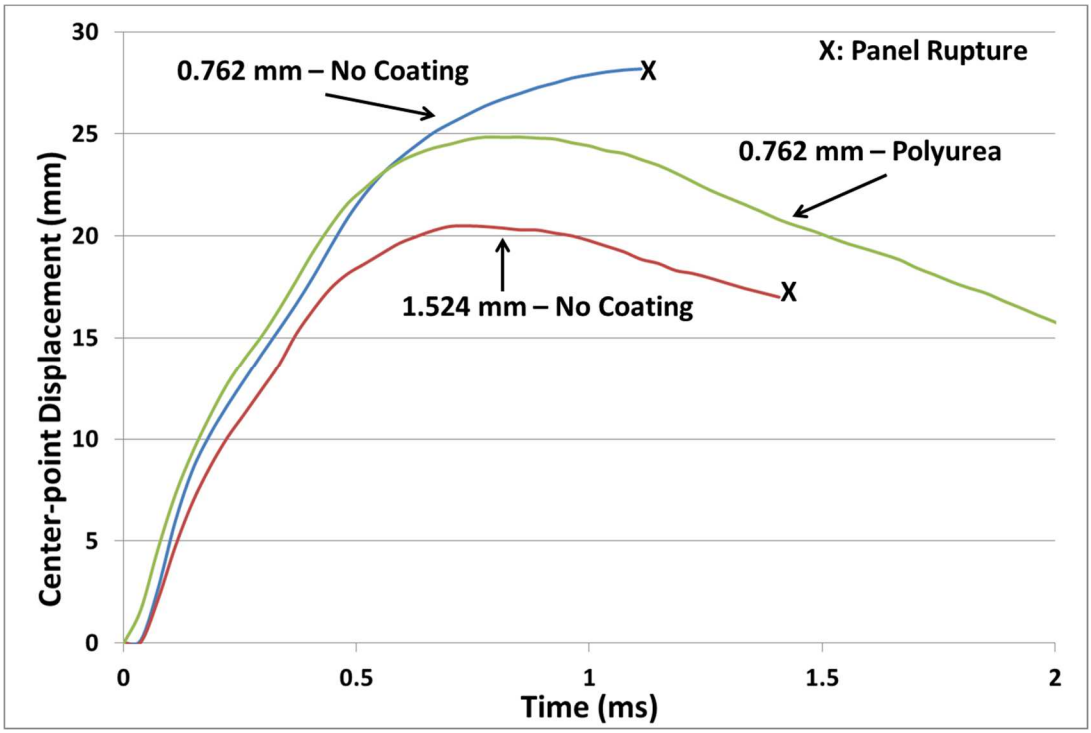

Figure 9: Plate center-point deflections

The deformation history of the baseline 0.762 mm uncoated composite plate as measured along a horizontal cut though the center of the plate is shown in Figure 10. The deformed profile plotted throughout time is illustrative of the deformation mechanics of the composite plate. From this figure it is seen that for a plate subjected to a centralized near field UNDEX loading, the deformation is initially dominated by localized deflections at the center with minimal deflection near the boundaries. As the plate responds to the pressure loading, it gradually transitions to an overall plate flexure mode as shown by the cross sectional shape at 0.63 and 1.11 ms. At 1.11 ms the plate experiences significant edge tearing and further observations of the plate deformation mechanics would be invalid due to partial rigid body motion of the plate. The significant observation is that the initial plate deformation is governed by the

highly localized pressure loading and then subsequently shifts to a mode I flexure deformation profile later in time.

The full-field displacement profiles for the back-face of each plate configuration are provided in Figure 11. The localized center-point deflection can be visualized in the 0.37 ms time frame and is consistent with the cross sectional shape plot, Figure 10. Furthermore the overall flexural deformation mode at 1.11 ms is clearly visible in the contour plots. Each of the three panel configurations exhibit similar deformation along their centerline with the primary difference being the magnitude of the displacement itself.

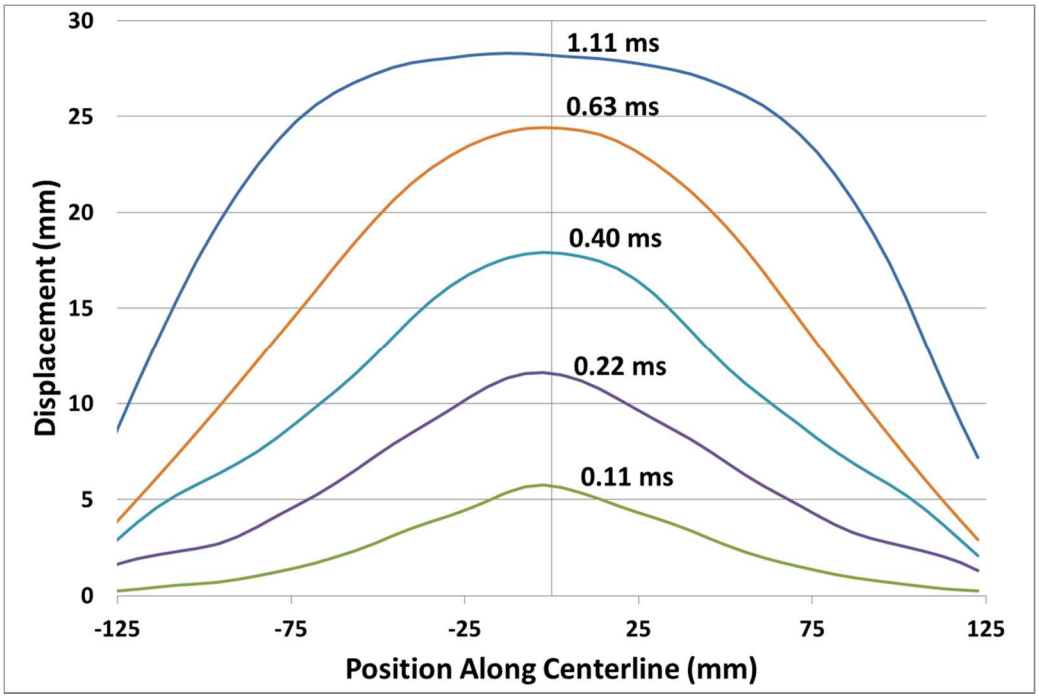

Figure 10: Plate Deformation - Horizontal Centerline

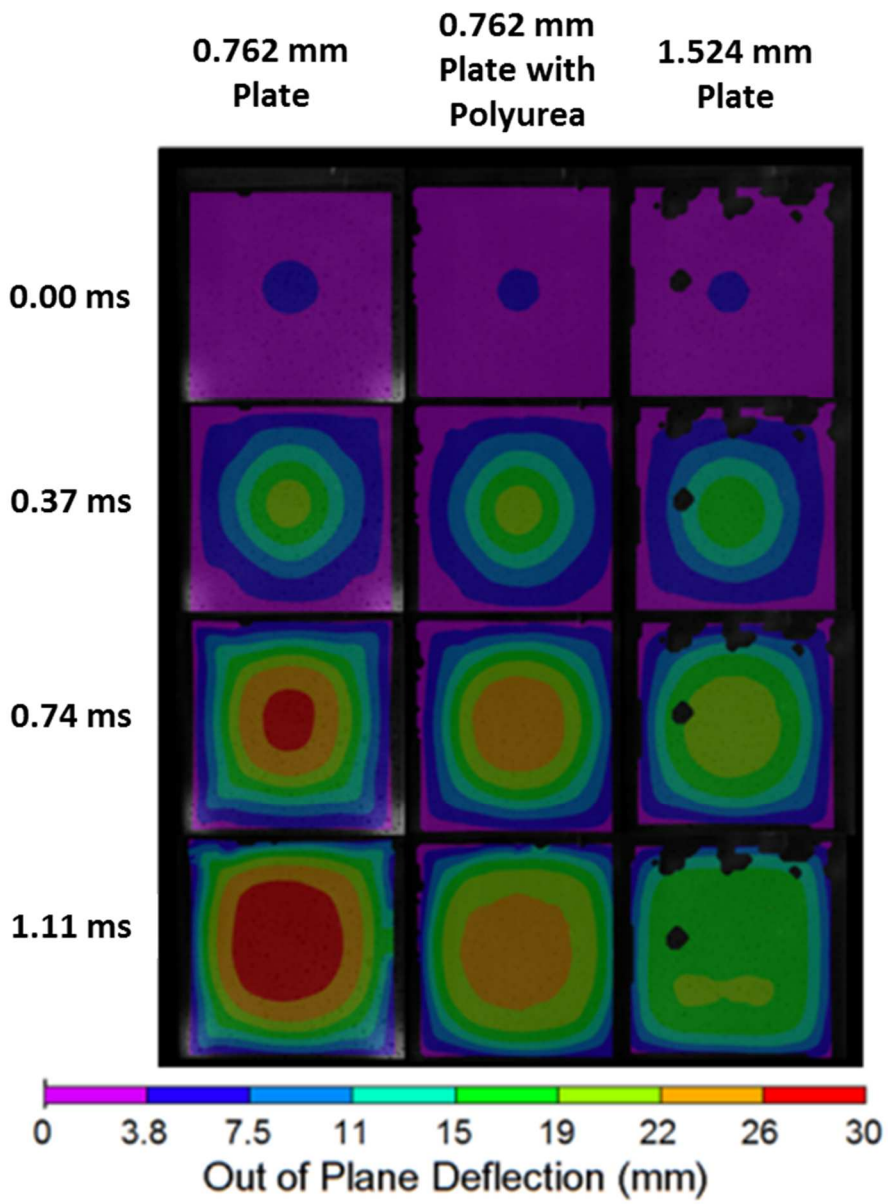

Figure 11: Full-Field Deflection Contours

The transient displacement results discussed thus far indicate a performance advantage when the thickness of the baseline plate is increased, or alternatively a polyurea coating is applied to the surface of the plate. However, when the plate thickness is increased or a coating is applied there is an associated penalty in that the plate weight is correspondingly increased. One means of quantifying the added mass

penalty in terms of transient deflection of the respective plates is to establish an Areal Weight Ratio (AWR) between the plate configurations [13]. The AWR is calculated by Equation 1

$$AWR = \frac{W_{2,3}}{W_1} \qquad (1)$$

where W_1 is the areal weight of the uncoated 0.762 mm composite baseline plate and $W_{2,3}$ is the areal weight of the polyurea coated 0.762 mm plate and the and 1.524 mm specimens, respectively. The AWRs for the 1.524 mm plate and the polyurea coated plate are 2 and 1.57 (Table 2). The AWR is subsequently employed as a multiplier applied to the transient center-point deflection data. The displacement data that has been adjusted (raw data multiplied by AWR) to account for the areal mass increase is shown in Figure 12. This plot shows that when the displacements are adjusted to account for the increased areal weight, the baseline plate outperforms both the thicker and polyurea coated plates. The normalized deflection of the polyurea coated specimen was 37.9% greater than the uncoated 0.762 mm specimen, and that the normalized deflection of 1.524 mm specimen was similarly 45.4% greater. This suggests that the additional laminate plies and the employed polyurea regime serve to degrade the deflection performance of the plate specimen with respect to AWR. This observation is consistent with previous findings for curved polyurea composite plates subjected to far field UNDEX loading in which polyurea coatings have been seen to result in larger AWR adjusted deflections [13]. It is noted that in the previous study, multiple coating thicknesses were considered and it was found that there are coating thicknesses for which the coated plate outperforms the baseline plate, even when

accounting for the AWR penalty. Thus, the findings of the single coating thickness considered in the current study do not preclude the existence of a polyurea coating thickness for composite plates subjected to near field UNDEX loading that both outweighs the weight penalty while also improving the deflection performance. Further work is needed to identify such a regime in the future. Finally, the 1.524 mm plate and 0.762 mm polyurea coated plates have approximately the same relative performance in terms of adjusted peak displacement when the added mass penalty is taken into consideration.

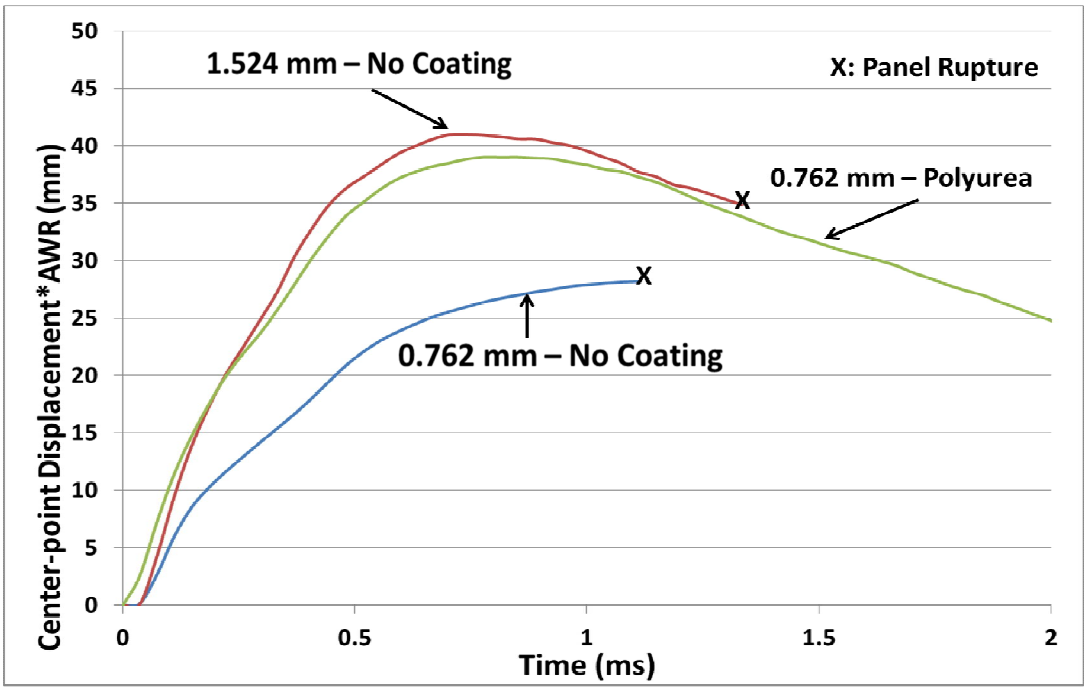

Figure 12: Areal Weight Adjusted Deflections

Table 5: Normalized plate center-point deflection results

Plate	Maximum AWR Deflection
0.762 mm	28.2 mm
0.762 mm (Coated)	38.9 mm
1.524 mm	41.0 mm

Summary and Conclusions

The response of submerged, air backed E-Glass / Epoxy composite plates, including polyurea coatings, when subjected to near field underwater explosive loading has been studied through experimentation and in the published work, computational modeling. The focus of the work is on determining how the response of a composite plate subjected to UNDEX is influenced by increased plate thickness or through the application of an elastomeric coating to the baseline plate. A water filled blast tank has been used to impart UNDEX loading to the composite plates in a controlled manner. The Digital Image Correlation system is used to capture the full-field, transient response of the back surface of the plates.

In the study the response of three unique plate configurations is studied: (1) 0.762 mm baseline plate, (2) 1.524 mm plate, and (3) 0.762 mm plate with a 0.762 mm polyurea coating applied to the back-face. Performance of the plate configurations is evaluated using the center-point and full-field time histories of the deflection of the back-face of the plates, as well as level of material damage. The experimental results show several effects on the transient response of the plates based on configuration. The use of a plate two times as thick as the baseline plate reduces the center-point defection by 27% while the application of a polyurea coating equal in thickness to the baseline plate results in a 12% deflection decrease. Additionally, the

polyurea coating is effective in reducing material damage as compared to both the baseline and thicker uncoated plates. Thus, when considering a plate design, the desired performance metric of the plate response should be considered. A thicker plate of structural material (composite) is preferable to reduce center-point deflection, while the use of polyurea coating is effective in reducing overall damage. However, in the case of an existing design the use of polyurea coatings can be an effective retrofitting application to improve the blast resistance of a structure while reducing overall material damage. Furthermore, it has been shown that through the use of an Areal Weight Ratio, there is a tradeoff between increased panel weight and mechanical performance. Although, both the thicker composite plate and the coated plate outperform the baseline plate, this performance increase comes at a penalty of increased weight. Thus if weight is a strong consideration in a specific application then maximum blast resistance may not be achievable and a relative tradeoff between weight and performance must be considered.

The computational model, documented in the published work demonstrated excellent correlation. The models are able to accurately simulate the detonation of the explosive charge and the resulting pressure fields and plate deflections.

Acknowledgements

The financial support of the Naval Undersea Warfare Center (Division Newport) In-house Laboratory Independent Research program (ILIR) directed by Neil Dubois is greatly acknowledged. The support of Dr. Y.D.S. Rajapakse of the Office of Naval Research under Grant Nos. N00014-10-1-0662 (University of Rhode Island)

and N00014-14-WX00730 (Naval Undersea Warfare Center, Division Newport)) is acknowledged.

References

[1] Latourte, F., Gregoire, D., Zenkert, D., Wei, X., Espinosa, H., "Failure Mechanisms in Composite Plates Subjected to Underwater Impulsive Loads", Journal of the Mechanics and Physics of Solids 2011; 59:1623-1646

[2] Espinosa, H., Lee, S., Moldovan, N., "A novel fluid structure interaction experiment to investigate deformation of structural elements subjected to impulsive loading". Experimental Mechanics 2006. 46 (6), 805–824.

[3] Schiffer, A., Tagarielli, V., " The Response of circular composite plates to underwater blast: Experiments and Modeling", Journal of Fluids and Structures 2015 52: 130-144

[4] Avachat, S., Zhou, M., "Response of Cylindrical Composite Structures to Underwater Impulsive Loading", Procedia Engineering 2014 88: 69-76

[5] Avachat, S., Zhou, M., "High-speed digital imaging and computational modeling of dynamic failure in composite structures subjected to underwater impulsive loads" International Journal of Impact Engineering 2015 77:147-165

[6] LeBlanc J, Shukla A. "Dynamic Response and Damage Evolution in Composite Materials Subjected to Underwater Explosive Loading: An Experimental and Computational Study" Composite Structures 2010 92:2421-2430

[7] LeBlanc J, Shukla A. “Dynamic Response of curved composite plates to underwater explosive loading: Experimental and computational comparisons” Composite Structures 2011 93:3072-3081

[8] Franz T, Nurick G, Perry M “Experimental investigation into the response of chopped-strand mat glassfibre laminates to blast loading” International Journal of Impact Loading 2002 27:639-667

[9] Mouritz AP “The effect of underwater explosion shock loading on the fatigue behaviour of GRP laminates” Composites 1995 26:3-9.

[10] Dear, J., Brow, S., “Impact Damage Processes in Reinforced Polymeric Materials”, Composites Part A: Applied Science and Manufacturing 2003 34:411-420

[11] Hodge N. Military experimenting with ‘Spray On’ armor for humvees, Defense Today 2004; 25

[12] LeBlanc, J., Shukla, A. “Response of Polyurea Coated flat composite plates to underwater explosive loading”, Journal of Composite Materials, Article in Press DOI: 10.1177/0021998314528263

[13] LeBlanc J, Gardner N, Shukla A. Effect of polyurea coatings on the response of curved e-glass / vinyl ester composite plates to underwater explosive loading. Compos: Part B 2013; 44: 565-574

[14] Tekalur SA, Shukla A, Shivakumar K. Blast resistance of polyurea based layered composite materials. Compos Struct 2008; 84: 271-281

[15] Gardner N, Wang E, Kumar P, Shukla A. Blast mitigation in a sandwich composite using graded core and polyurea interlayer. Exp Mech 2012; 52:119-133

[16] Amirkhizi A, Isaacs J, McGee J, Nemat-Nasser S. An experimentally-based viscoelastic constituitve model for polyurea, including pressure and temperature effects. Phil Mag 2006; 86: 5847-5866

[17] Amini MR, Isaacs JB, Nemat-Nasser S. Experimental investigation of response of monolithic and bilayer plates to impulsive loads. Int J of Impact Eng 2010; 37: 82-89

[18] Amini MR, Simon J, Nemat-Nasser S. Numerical modeling of effect of polyurea on response of steel plates to impulsive loads in direct pressure-pulse experiments. Mech Mater 2010; 42: 615-627

CHAPTER 3

CONFINED HYDROSTATIC IMPLOSION OF PMMA CYLINDRICAL TUBES

by

Christopher Shillings, Sachin Gupta, Arun Shukla

Prepared for submission to Experimental Mechanics

Corresponding Author: Christopher Shillings

University of Rhode Island

Mechanical, Industrial and Systems Engineering

92 Upper College Road, Kingston, RI 02881

Phone: 401 – 864 – 9443

Email Address: shill52@my.uri.edu

Abstract

An experimental investigation is conducted to study the underwater implosion of brittle materials under hydrostatic pressure. The cylindrical volumes (implodables) chosen in this study are polymethylmethacrylate (PMMA) tubing. Three geometries of tubing were chosen with an outer diameter of 25.4 mm and wall thickness of 1.59 mm with varying lengths of 76.2 mm, 152.4 mm and 228.6 mm. Implodable volumes are centrally placed and suspended concentrically about the length of a horizontal, tube shaped confining vessel. The evaluation of buckling and fracture in the confining vessel is captured using high-speed photography and dynamic pressure sensors are utilized to record pressure histories during and after the implosion event. From experimental images all geometries of implodables display distinct dynamic crack patterns leading to fluid penetration and catastrophic failure of the PMMA structure.

From experimental results, the confined vessel plays a significant role in diminishing the damage potential of pressures often seen in free field implosions. With an increase in implodable tube volume, hydrostatic pressure is drastically reduced during and after an implosion, further reducing pressure increases within the confined region. Pressure history results in this study show good agreement with a previous study of the confined hydrostatic implosion of aluminum cylindrical tubes.

Introduction

A comprehensive series of experiments is preformed to understand the implosion characteristics of PMMA tubing within a confined vessel. The primary purpose of this study is to characterize brittle tube implosion by means of high-speed photography. Additionally, pressure history will be recorded during the implosion. Images and pressure histories are synchronized to give a clear depiction of the implosion event.

The motivation for brittle tube implosion research stems from the use of brittle materials in naval applications. Since the dynamic buckling of shell structures is very catastrophic, the coupled brittle behavior inspires a search to understand such a highly transient and complex event. Through brittle implosion research the goal is to identifying, the origin of failure and failure mechanisms in the brittle structure.

Under critical hydrostatic pressure, a fully encapsulated volume containing a low-pressure gas can buckle. If the collapse is rapid enough, the change in momentum of the fluid discharges a high-pressure acoustic wave which poses a threat to structures in the vicinity of the implosion [1-10]. Extensive work has been accomplished in the field of implosion, primarily with the focus of understanding the pressures emitted from the buckled structure, but little to no work has been done to study the development of cracks during the implosion of brittle materials.

This paper will discuss the implosion of PMMA tubing, failure origins and mechanisms of failure. From experimental results, it can be determined that there are distinct crack patterns of failure during brittle implosion.

Specimen and Material Studied

The material chosen in this study is polymethylmethacrylate (PMMA). Three geometries of PMMA tubing are chosen to compare how variation in length alters the implosion behavior. These geometries are listed in Table 1 with additional information about the tubes such as: each implodable's volume (V_i), implodable to confined vessel ratio (V_i:V_{cv}) and theoretical implosion pressures.

Table 1: Implodable geometries and critical implosion pressure

Geometry	Unsupported Length (l)	Outer Diameter (d)	Wall Thickness (t)	Unsupported Implodable Volume (V_i)	V_i:V_{cv}	Theoretical Critical Pressure (P_{cr})
I-SL	76.2 mm	25.4 mm	1.59 mm	29.57 ml	1:1900	3.04 MPa
I-ML	152.4 mm	25.4 mm	1.59 mm	59.14 ml	1:950	2.41 MPa
I-LL	228.6 mm	25.4 mm	1.59 mm	88.71 ml	1:630	2.35 MPa

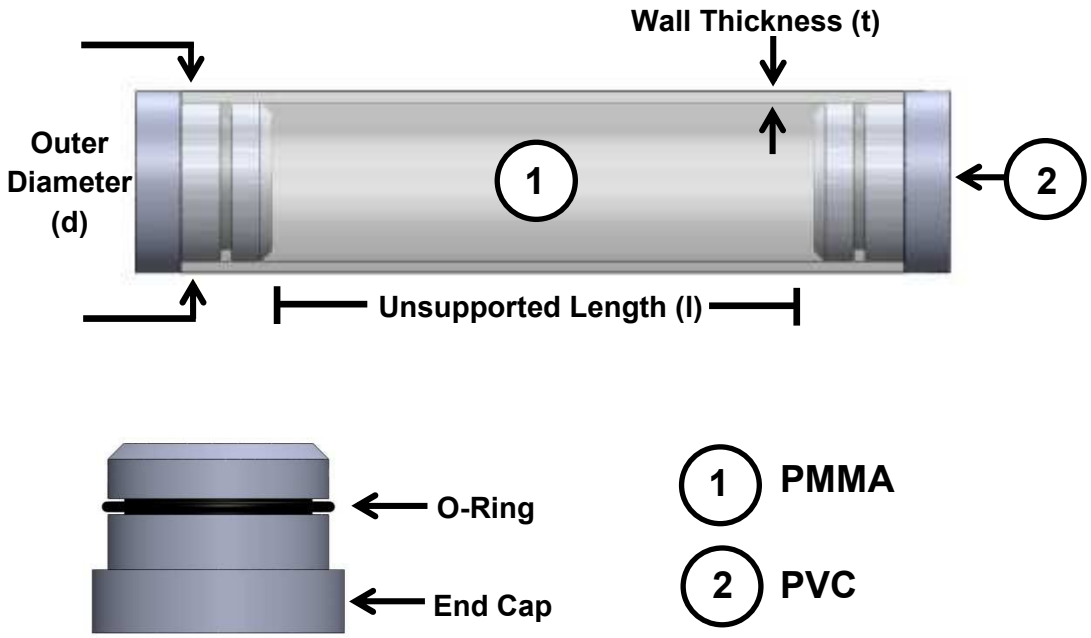

Figure 1: Specimen Assembly

Each implodable is capped at their ends with specially designed end caps. The end caps are made of PVC plastic and fashioned with O-Rings for a watertight seal. In

addition to O-Rings, fast setting epoxy is applied to the end cap, tube interface for additional sealant. A schematic of the assembly is shown in Figure 1.

Experimental Setup and Methods

A complete summary of experimental methods is published in the journal paper, Mechanics of the Implosion of Cylindrical Shells in a Confining Tube by Sachin Gupta et al.

Confining Vessel with Viewing Window

The Confining Vessel in Figure 2 is an apparatus created to provide a finite region in which an implosion can be documented by high-speed photography and pressure data collection. The Confining Vessel is a thick-walled, steel tube with an internal diameter of 17.78 cm (7”), wall thickness of 1.91 cm (¾”) and a total internal length of 228.6 cm (90”). Mounted about a steel I-Beam for stability, the vessel can withstand internal pressures up to 10.34 MPa (1500 psi) supplied by an external pressurization unit.

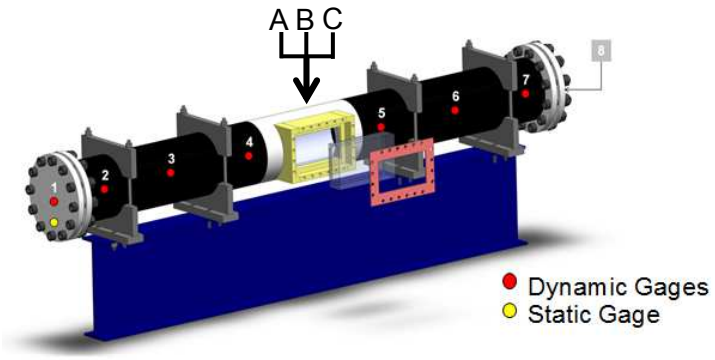

Figure 2: Confined Vessel

High-speed photography of the implodable is accomplished through the viewing window positioned at the center of the vessel. The window section consists

of a clear acrylic slab 26.67 cm x 15.24 cm (10.5" x 6") compressed to a rectangular porthole by a steel frame and sealed about the vessel interface with an o-ring. The metal frame reduces the viewing area to 22.86 cm x 11.43 cm (9" x 4.5").

The Confining Vessel is also equipped with eleven piezoelectric, dynamic pressure gages, which are flush mounted about the vessel wall and located about its total length. These sensors are responsible for capturing the pressure fluctuations caused by the implosion. The positioning and numbering of the gages are presented in Figure 1 and 2

Specimen Setup in Confining Vessel

The specimen's mounting fixture is shown in Figure 3. In order to keep the PMMA specimen concentric within the confined vessel aluminum collets with rubber coated spokes were created. The spokes are rubber coated to maintain the centered axial location in the confined vessel while filling with water and during the implosion event. In Figure 3 the axial view labels the viewing window used for high speed photography.

Camera Setup and Imaging

The camera used for experimentation is the Photron SA1.1. The Photron is used to capture the implosions at frame rates up to 54,000 fps. The lighting fixtures used for the photography are the Frezzi Super Sun Gunn 400s. Figure 4 displays the viewable area of the camera along with an experimental image of geometry 1 prior to applying hydrostatic pressure above ambient conditions. In the experimental image two streaks of light can be seen along the length of the specimen. The streaks are

refracted light due to the curved PMMA tube's surface; however this distortion of light does not interfere with the implosion event.

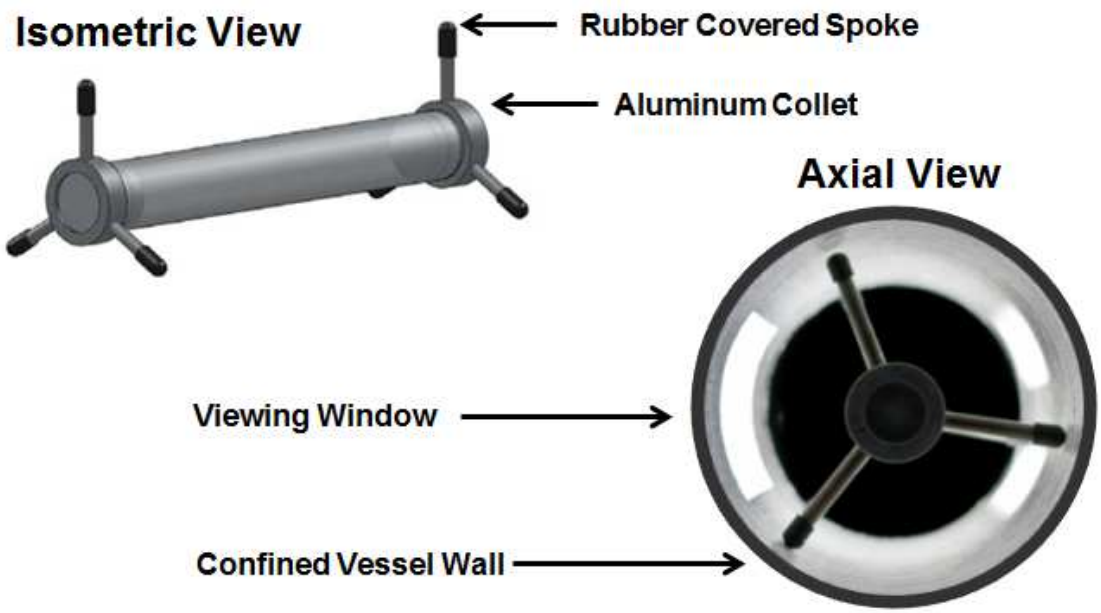

Figure 3: Specimen mounting fixture

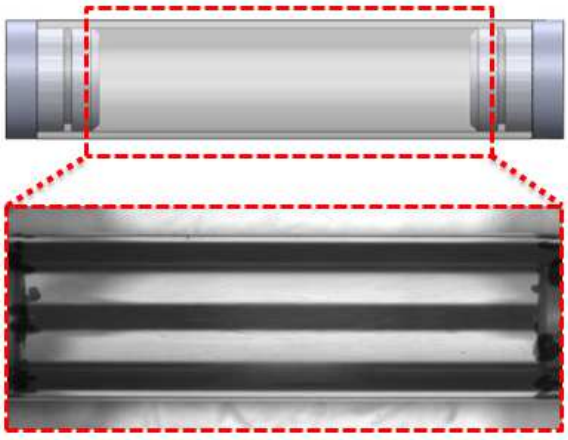

Figure 4: High Speed Photography Resolution

Although there are optical difficulties associated with the translucent specimens, the clarity allows for the observation of crack formation and propagation.

Results

Pre-Implosion Behavior

Before any brittle failure there is an observable deformation about the tube cross section. Figure 5 is a CAD schematic of the deformation from two perspectives prior to implosion. While the camera remains stationary, the tube is free to deform. The deformation occurs as ovaling about the cross section of tube with the maximum deflection about the center of the free length. Figure 5 shows what will be described as the 0˚ and 90˚ perspectives.

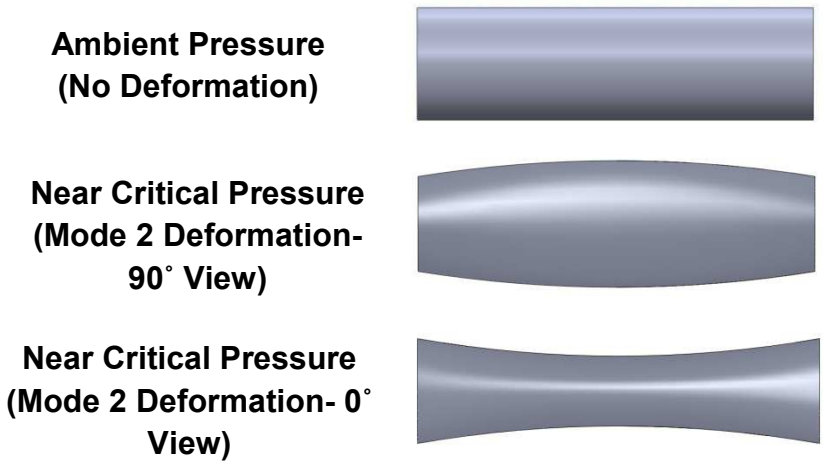

Figure 5: Pre-Implosion deformation due to near critical hydrostatic pressure

Figure 6 displays the pre-implosion behavior of the tube from experimental images. Both the second and third rows of the figure are images from two different experiments to show the 0˚ and 90˚ deformation perspectives. From the experimental images the curvature of the refracted light serves as a key indicator of this buckling behavior. All tube geometries experience mode two deformation before imploding.

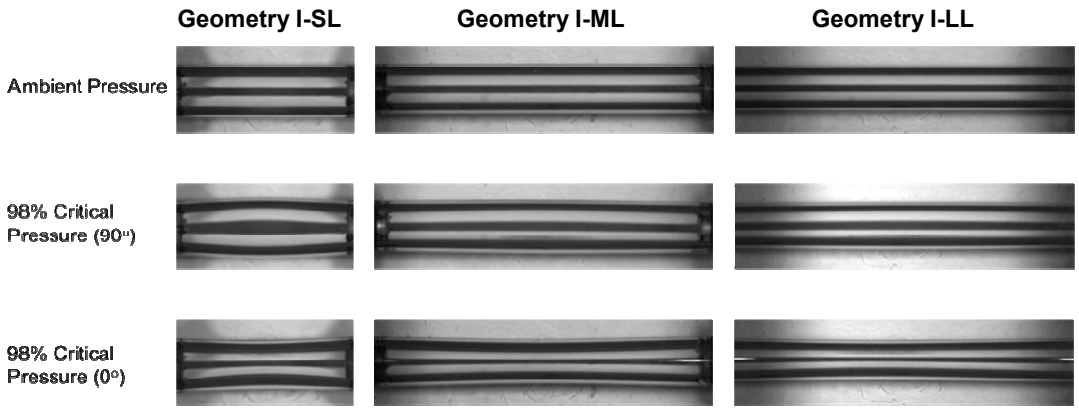

Figure 6: Deformation prior to brittle implosion

Implosion Behavior

During the implosion event, all geometries display similar cracking behavior leading to fluid penetration and the overall destruction and fragmentation of the PMMA tube. Although distinct, dynamic cracking patterns occur amongst all geometries, all geometry's crack progression time is geometrically dependent.

Figure 7 is a schematic of a PMMA crack progression under specimen under hydrostatic loading. The figure includes two perspectives, 0° and 90° to give a full understand of where and how the cracks form and progress. The primary crack is the first crack to form occurring at one of the highly curved regions of the tube, while the secondary cracks forms later in time after the primary crack has fully propagated. Figure 6 shows within less than 0.5 ms of the primary crack forming, the crack progression throughout time.

Once the curvature of the PMMA tube reaches a critical pressure the primary crack forms and propagates about the length of the specimen causing the opposing

tube walls to collapse radially. Typically the primary crack forms on one surface of the tube, however there have been instances of two primary cracks forming in unison. When the primary crack is driven until it reaches the end caps, secondary cracks form approximately 90˚ from the primary crack with respect to the circumference of the tube. Secondary cracks form 180° from each other. The secondary cracks, forming on both the front and back face of the tube rapidly bifurcate and fluid typically penetrates the secondary crack region leading to a rapid drop in hydrostatic pressure.

In this study brittle implosion is documented to be a highly complex, transient event. In Figures 8, 9 and 10 the experimental images for each implosion are coupled with their appropriate pressure history recorded at pressure sensor B. The dynamic pressure of each implosion is plotted versus time in milliseconds. Images B through D are the full dynamic crack progression, before fluid penetration.

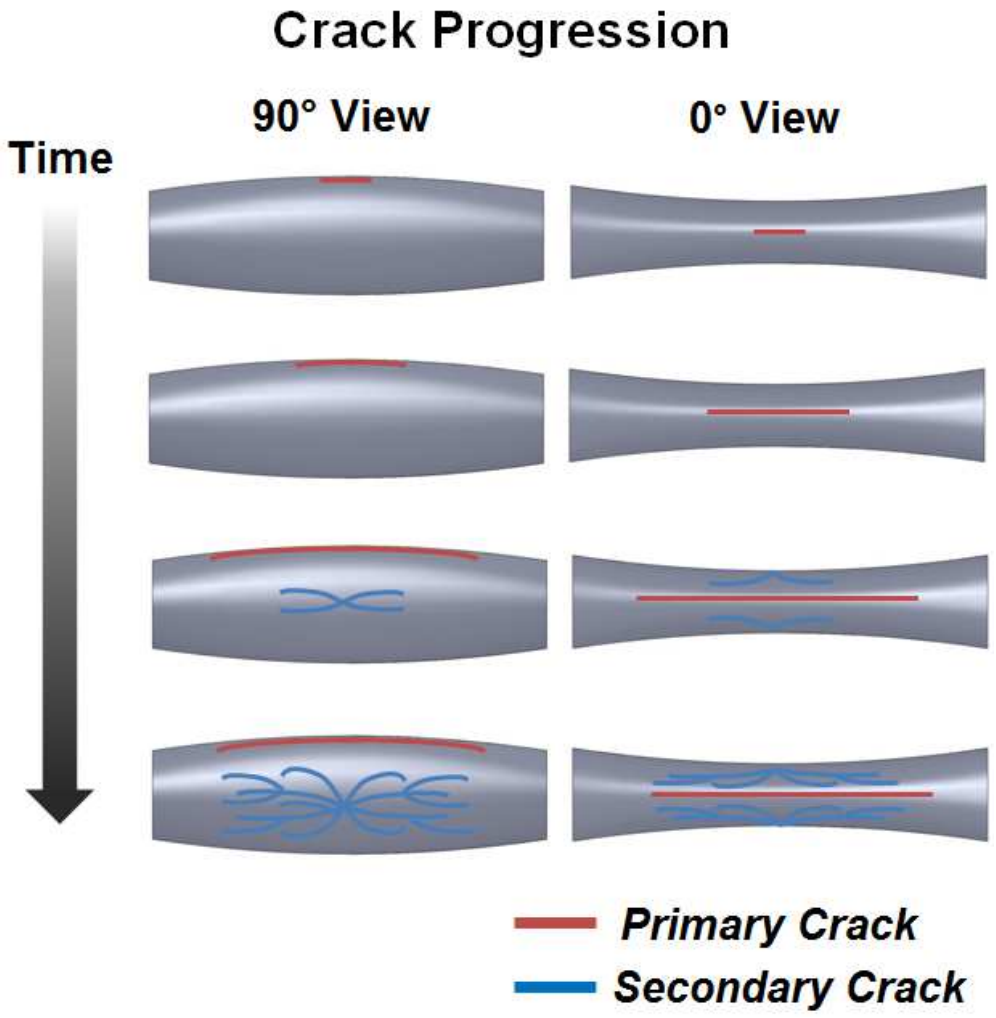

Figure 7: Dynamic Crack Progression in PMMA Tubing

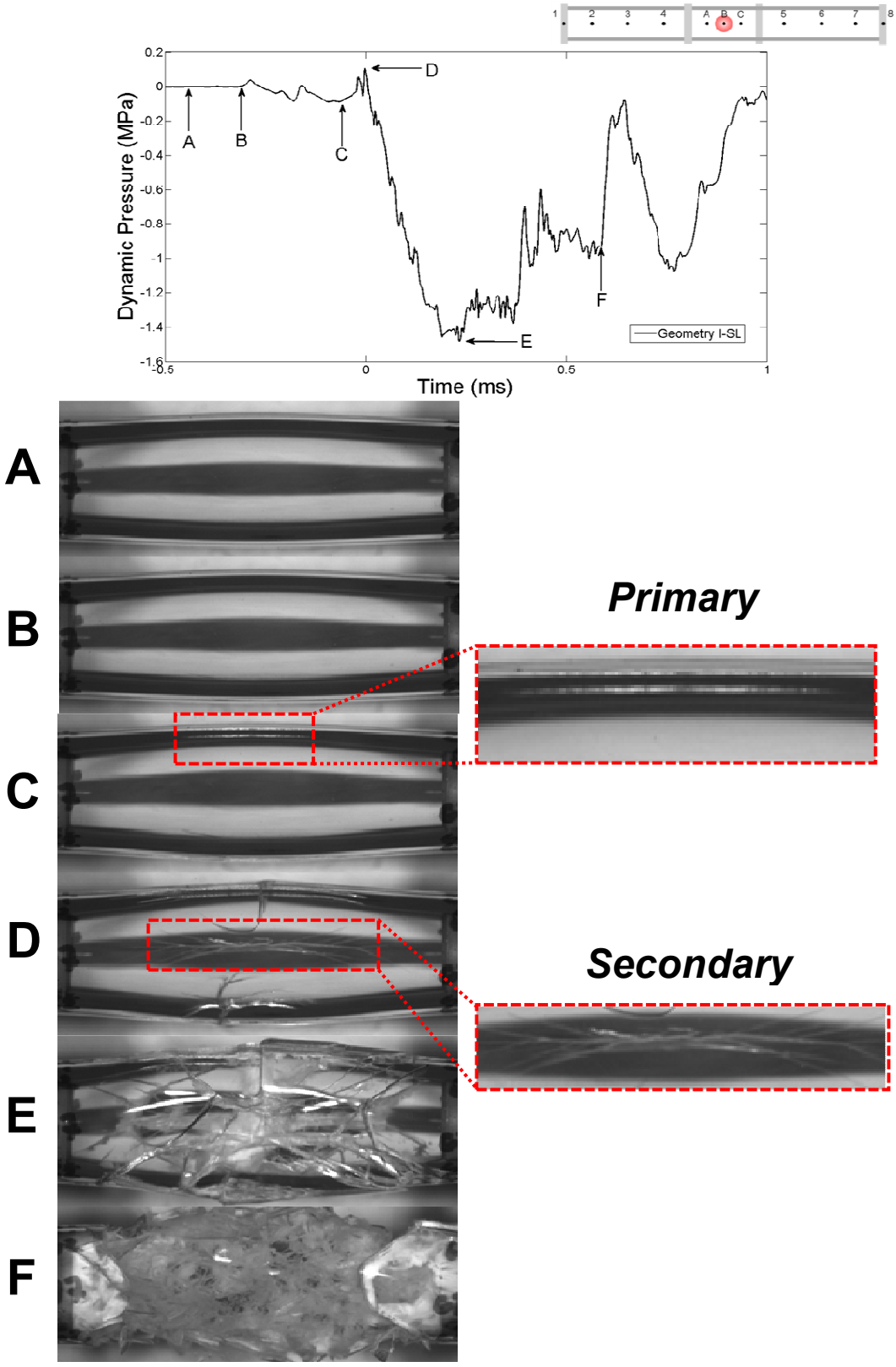

Figure 8: High Speed Images and Pressure History of Geometry I-SL

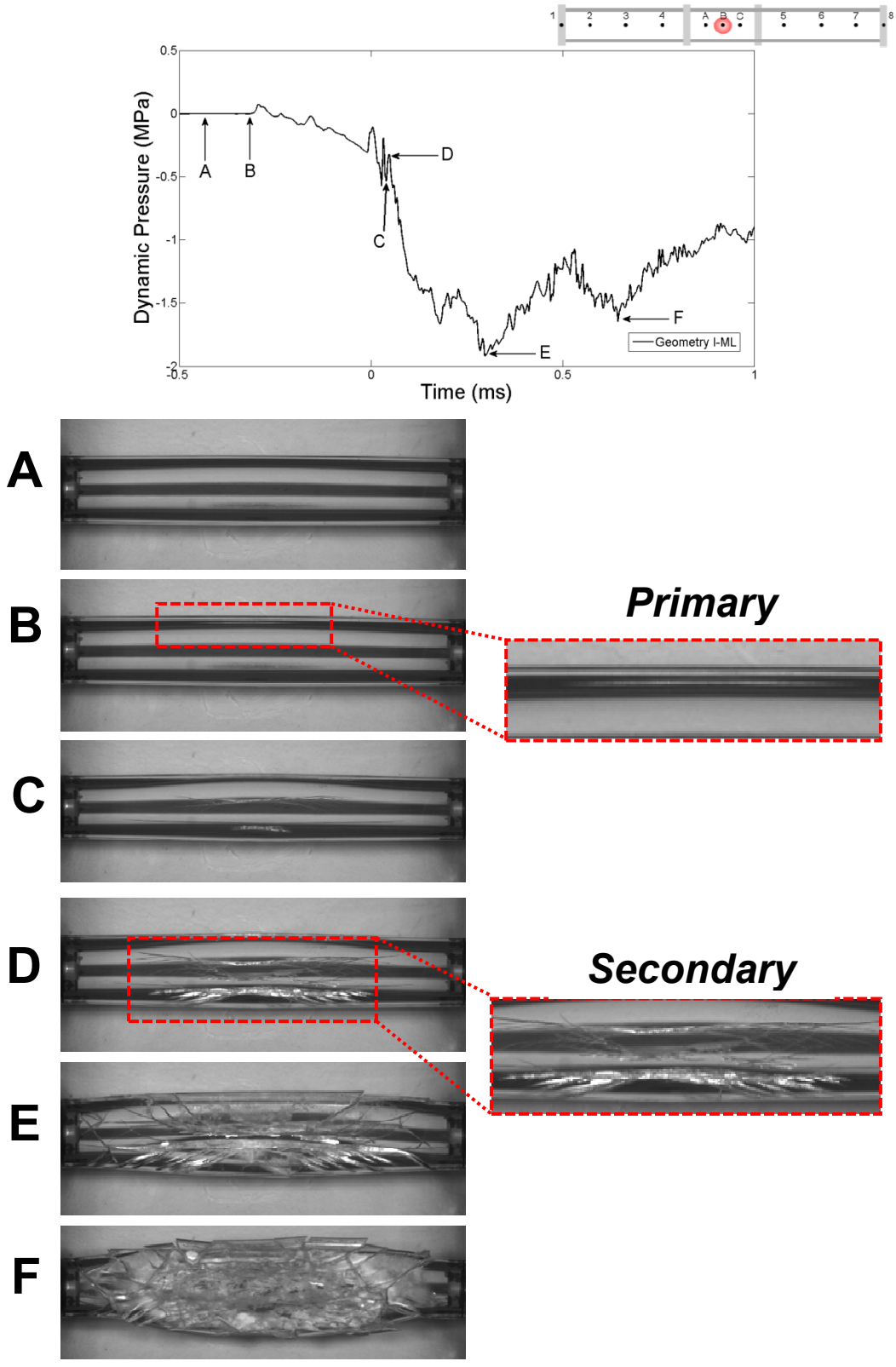

Figure 9: High Speed Images and Pressure History of Geometry I-ML

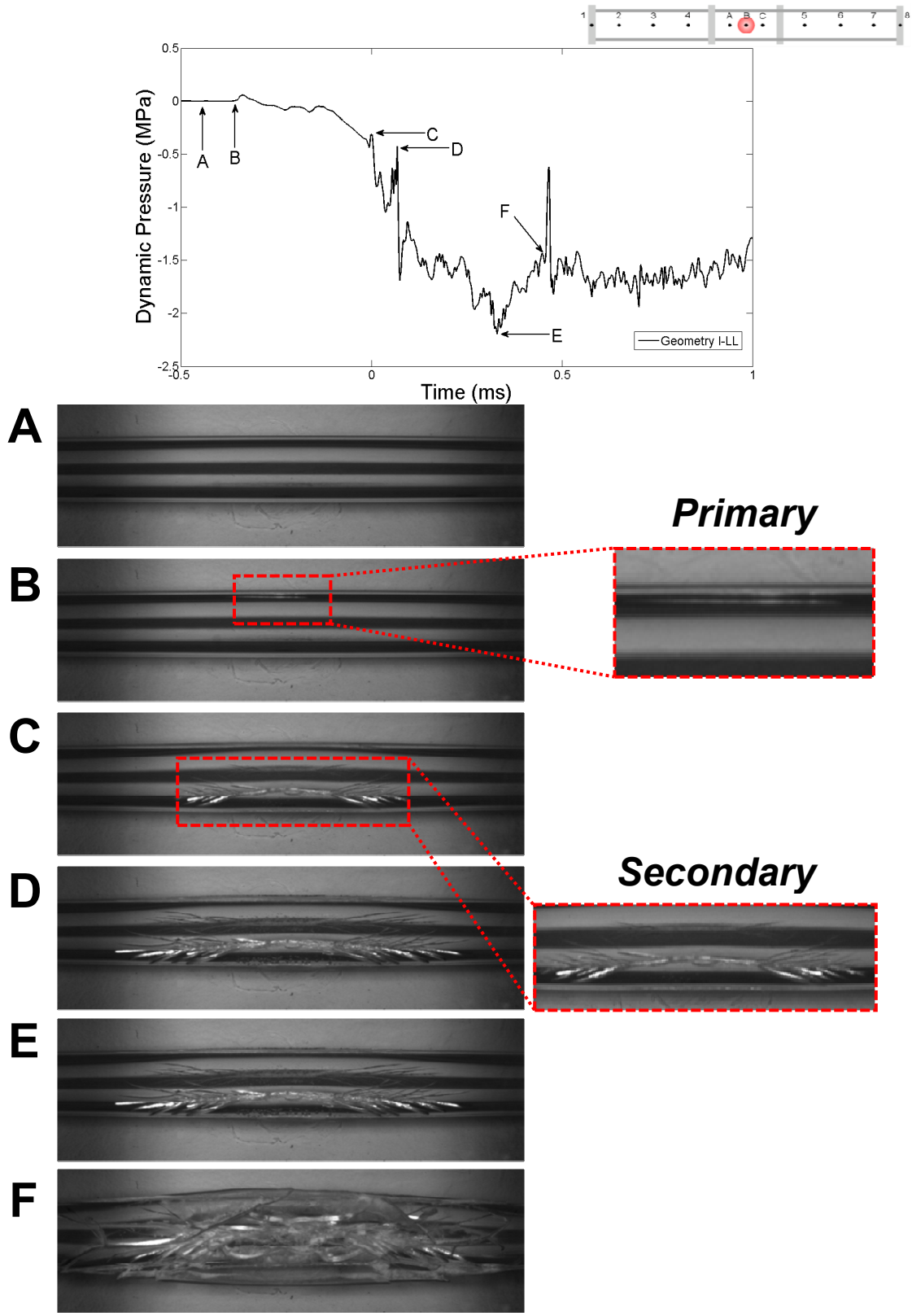

Figure 10: High Speed Images and Pressure History of Geometry I-LL

Primary crack progression

Documenting the initial dynamic behavior of the primary crack was limited to a few frames. Figure 11 is a plot of the axial crack distance (total primary crack length divided by two) versus time in milliseconds. The estimated initial crack speed is measured to be from 600 to 700 m/s, about ~ 50% to 60% of the material's Rayleigh Wave Speed of PMMA.

In previous dynamic crack studies by Dally, it is mentioned that the theoretical maximum crack velocity in a material is the Rayleigh wave velocity. Nonetheless, this velocity is typically not achieved because the energy driving the crack is divided in bifurcation [11].

In work published by Shukla et al. it was analytically determined that the addition of a superimposed compressional load parallel to the crack suppresses crack bifurcation. The energy inducing crack growth is then focused into the growth of the crack, increasing the velocity of the crack tip [12].

With regard to the superimposed compressional load parallel to the crack direction, Dally studied the velocity of cracks after detonation of a small explosive centrally placed in a hole located in Homalite 100. The Homalite 100 confining the explosive created a radial compression in the material. After detonation, cracks formed and propagated radially in the direction of the superimposed compression at 726 m/s, about 56% of the material's Rayleigh Wave speed. As the cracks extended the velocities decreased and the cracks later bifurcated [11].

In the study of the implosion of PMMA tubes, the tube experiences a global compressive loading because of hydrostatic pressure. The primary crack from the pre-

implosion deformation is formed as a mode one crack and is driven in the direction of the compressive load, resulting in suppression of bifurcation and causing initial primary crack velocities of 600 to 700 m/s.

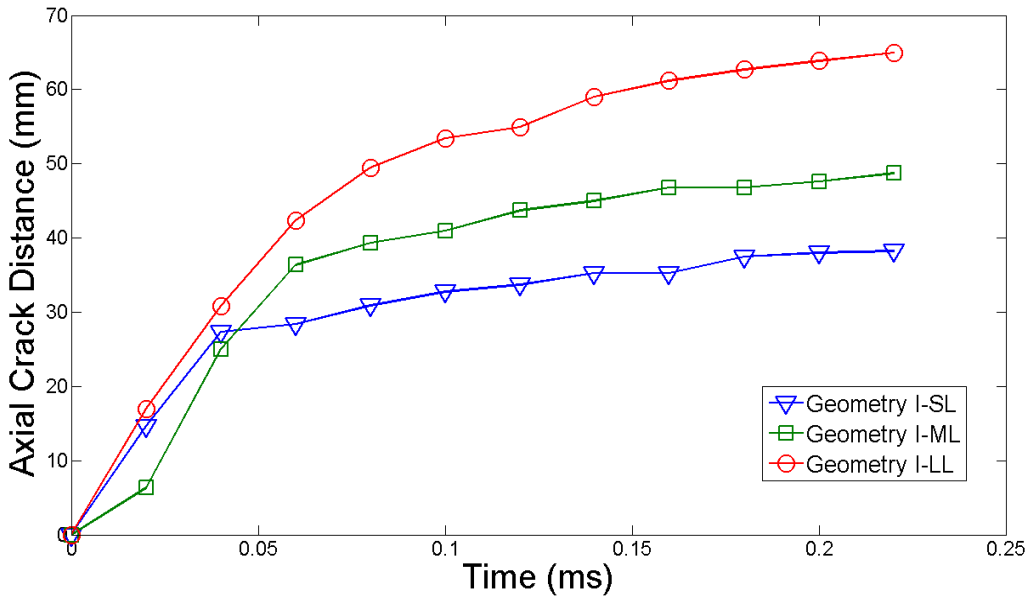

Figure 11: Primary crack propagation distance versus time

Pressure History

Due to dynamic fracture of the specimen, pressure history appears to display acoustic signals however this high frequency fluctuation in pressure is most likely due to acoustic discharge from the brittle implosion. This write up does not go into the detail of the pressure history, but a complete description of the confined vessel pressure dynamics is published in the journal paper, Mechanics of the Implosion of Cylindrical Shells in a Confining Tube by Sachin Gupta et al. This work looks into the confined implosion of ductile material, discussing the reduction in pressure produced by an implosion due to the confined boundary condition.

Conclusions

- All specimen geometries display a distinct deformation and crack patterns during the implosion event
    - Specimens oval in mode 2 prior to crack formation
    - Initial primary crack speeds range between 600 m/s to 700 m/s
    - Secondary cracks form 90˚ from the primary crack causing the degradation of the structure leading to fluid penetration
- Local pressure history shows a similar decrease in hydrostatic pressure during implosion, similar to previous implosion work in a confined pressure vessel
    - Pressure history displays high frequency most likely due to noise from the dynamic fracture event

Acknowledgements

The authors kindly acknowledge the financial support provided by the Office of Naval Research Computational Mechanics Program managed by Dr. Stephen E. Turner under Grant No. N00014-12-1-0382.

References

[1] Dyau, J.y., and S. Kyriakides. "On the Propagation Pressure of Long Cylindrical Shells under External Pressure." *International Journal of Mechanical Sciences* 35.8 (1993): 675-713.

[2] Farhat, C., K.g. Wang, A. Main, S. Kyriakides, L.-H. Lee, K. Ravi-Chandar, and T. Belytschko. "Dynamic Implosion of Underwater Cylindrical Shells: Experiments and Computations." *International Journal of Solids and Structures* 50.19 (2013): 2943-961.

[3] Gupta, Sachin, James M. Leblanc, and Arun Shukla. "Mechanics of the Implosion of Cylindrical Shells in a Confining Tube." *International Journal of Solids and Structures* 51.23-24 (2014): 3996-4014.

[4] Gupta, Sachin, Venkitanarayanan Parameswaran, Michael Sutton, and Arun Shukla. "Application of 3-D Digital Image Correlation Technique to Study Underwater Implosion." *Dynamic Behavior of Materials, Volume 1 Conference Proceedings of the Society for Experimental Mechanics Series* (2014): 351-56.

[5] Kyriakides, S., and C. D. Babcock. "Experimental Determination of the Propagation Pressure of Circular Pipes." *Journal of Pressure Vessel Technology J. Pressure Vessel Technol.* 103.4 (1981): 328.

[6] Leblanc, James, J. Ambrico, and S. Turner. "Underwater Implosion Mechanics: Experimental and Computational Overview." *Blast Mitigation* (2013): 161-87.

[7] Pinto, Michael, and Arun Shukla. "Dynamic Collapse Mode Evolution in Carbon Composite Tubes." *Extreme Mechanics Letters* 3 (2015): 55-58.

[8] Pinto, Michael, Sachin Gupta, and Arun Shukla. "Study of Implosion of Carbon/epoxy Composite Hollow Cylinders Using 3-D Digital Image Correlation." *Composite Structures* 119 (2015): 272-86.

[9] Turner, Stephen E., and Joseph M. Ambrico. "Underwater Implosion of Cylindrical Metal Tubes." *Journal of Applied Mechanics J. Appl. Mech.* 80.1 (2012): 011013.

[10] Turner, Stephen E. "Underwater Implosion of Glass Spheres." *The Journal of the Acoustical Society of America J. Acoust. Soc. Am.* 121.2 (2007): 844.

[11] Dally, James W. "Dynamic Photoelastic Studies of Fracture." *Experimental*

Mechanics 19.10 (1979): 349-61.

[12] Shukla, A., H. Nigam, and H. Zervas. "Effect of Stress Field Parameters on Dynamic Crack Branching." *Engineering Fracture Mechanics* 36.3 (1990): 429-38.